UTILIZING PACKED BED REACTORS FOR THE EMPLOYMENT OF C–H FUNCTIONALIZATION IN CONTINUOUS PROCESSING

A Dissertation
Presented to
The Academic Faculty

by

Taylor A. Hatridge

In Partial Fulfillment
of the Requirements for the Degree
Master of Science in the
School of Chemical and Biomolecular Engineering

Georgia Institute of Technology
May 2021

UTILIZING PACKED BED REACTORS FOR THE EMPLOYMENT OF C–H FUNCTIONALIZATION IN CONTINUOUS PROCESSING

Approved by:

Dr. Christopher Jones, Advisor
School of Chemical & Biomolecular Engineering
Georgia Institute of Technology

Dr. Fani Boukouvala
School of Chemical & Biomolecular Engineering
Georgia Institute of Technology

Dr. Stefan France
School of Chemistry & Biochemistry
Georgia Institute of Technology

Dr. Blair Brettmann
School of Chemical & Biomolecular Engineering
School of Materials Science & Engineering
Georgia Institute of Technology

Dr. Hang Lu
School of Chemical & Biomolecular Engineering
Georgia Institute of Technology

Date Approved: April 27, 2021

To those who have and who are continuing to redefine the aesthetic of science and engineering.

ACKNOWLEDGEMENTS

I would like to thank my collaborators: Dr. Chun-Jae Yoo, Dr. Wenbin Liu, Bo Wei, and Dr. Huw Davies. In particular, Wenbin and Bo taught me so much about the organic chemistry discussed in this thesis, which greatly enriched my graduate education.

Financial support for this work was provided by the National Science Foundation under the CCI Center for Selective C–H Functionalization (CHE-1700982). This material is also based upon work supported by the National Science Foundation Graduate Research Fellowship Program under Grant No. DGE-1650044. Any opinions, findings, and conclusions or recommendations expressed in this material are those of the author(s) and do not necessarily reflect the views of the National Science Foundation.

TABLE OF CONTENTS

ACKNOWLEDGEMENTS iv

LIST OF TABLES vii

LIST OF FIGURES viii

LIST OF SYMBOLS AND ABBREVIATIONS x

SUMMARY xii

CHAPTER 1. Introduction 1
1.1 Traditional organic synthesis and propensity for waste in the pharmaceutical industry 1
1.2 C–H functionalization and dirhodium carbenes 3
1.3 Challenges in industrialization of dirhodium carbene-mediated C–H insertion 6
1.4 Research Objectives 8

CHAPTER 2. implementation of immobilized dirhodium(II) carboxylate catalysts for C–H functionalization in a packed bed reactor 10
2.1 Background 10
2.1.1 Previous approaches to immobilize Rh_2L_4 catalysts and conduct C–H insertion in flow 10
2.1.2 Optimizing immobilization of $Rh_2(TPCP)_4$ catalysts on a mesoporous silica support (conducted by collaborators) 11
2.2 Materials and Experimental Methods 17
2.2.1 General Considerations 17
2.2.2 Synthesis of platelet SBA-15 19
2.2.3 $Rh_2(S\text{-}2\text{-}Cl\text{-}5\text{-}CF_3TPCP)_4$ catalyst immobilization and characterization 22
2.2.4 Hexamethyldisilazane-capped silica synthesis and characterization 26
2.2.5 General flow procedure for C–H insertion in a packed bed 27
2.3 Results and Discussion 29
2.3.1 Implementation of $Rh_2(S\text{-}2\text{-}Cl\text{-}5\text{-}CF_3TPCP)_4$ in a packed bed reactor 29
2.3.2 Process Performance 32
2.4 Conclusion 35

CHAPTER 3. Development of a catalytic process for aerobic oxidation of hydrazone compounds using a three-phase packed bed reactor 36
3.1 Background 36
3.1.1 Previous approaches to synthesize diazo compounds in flow 36
3.1.2 A catalytic method for hydrazone oxidation 37
3.1.3 Flow processes for aerobic oxidation 38
3.2 Materials and Experimental Methods 39
3.2.1 General Considerations 39

3.2.2 Split test 40
3.2.3 General flow procedures 41
3.3 Results and Discussion 45
3.3.1 Probing reaction conditions in batch 45
3.3.2 Optimizing the flow procedure 47
3.3.3 Characterization and packed bed performance 56
3.3.4 Semi-batch dirhodium(II) carbene reactions for immediate consumption of diazo intermediate 60
3.4 Conclusion 63

CHAPTER 4. Conclusions and Recommendations 64
4.1 Conclusions and broader impact 64
4.2 Recommendations for future work 67
4.2.1 Further investigation into the deactivation of the immobilized dirhodium(II) catalyst 67
4.2.2 Further improvements to the hydrazone oxidation process 70
4.2.3 Demonstrate scalability of C–H functionalization process 71

References 72

LIST OF TABLES

Table 1	The effect of tether location and catalyst nature on Rh_2(*S*-*o*-ClTPCP)$_4$ catalyst performance	15
Table 2	Characterization of platelet SBA-15	20
Table 3	Characterization of azido-grafted platelet SBA-15	24
Table 4	Effect of flow rate on catalyst performance	31
Table 5	Recyclability results for the immobilized Rh_2(*S*-2-Cl-5-CF_3TPCP)$_4$ catalyst	34
Table 6	Effect of DMAP on reaction performance	50
Table 7	Values for variables of interest in parameter space exploration	51
Table 8	Hydrodynamic regimes encountered at different air and liquid flow rates	55

LIST OF FIGURES

Figure 1	Traditional methods for organic synthesis rely on conversion of reactive functional groups	2
Figure 2	Illustration of general strategies to attain site selectivity in C–H functionalization reactions	4
Figure 3	Select examples of dirhodium(II) tetracarboxylate catalysts	5
Figure 4	General mechanism for dirhodium(II)-catalyzed C–H insertion reactions with diazo compound precursors	6
Figure 5	Chemical and crystal structures of Rh_2(*S*-*o*-ClTPCP)$_4$ catalyst	13
Figure 6	Homogeneous and heterogenized modified derivatives of Rh_2(*S*-*o*-ClTPCP)$_4$ catalyst	14
Figure 7	SEM and TEM images of regular SBA-15 and platelet SBA-15	16
Figure 8	Effect of SBA-15 mesopore length on reaction time and catalyst TOF	17
Figure 9	Adsorption and desorption isotherms and pore size distribution of platelet SBA-15 from cryogenic N_2-physisorption	21
Figure 10	SEM and TEM images of platelet SBA-15	21
Scheme 1	Preparation of Rh_2(*S*-2-Cl-5-CF_3TPCP)$_4$ immobilized catalyst	22
Figure 11	Characterization of azido-grafted platelet SBA-15 via TGA, IR, and cryogenic N_2 physisorption	24
Scheme 2	Synthesis of HMDS-capped hydrophobic silica surface	26
Figure 12	TGA curve for HMDS-grafted silica	27
Figure 13	Flow process diagram for C–H insertion continuous process	28
Figure 14	Substrate scope showing Rh_2(*S*-2-Cl-5-CF_3TPCP)$_4$ catalyst performance in flow and batch reactions	33
Figure 15	Raw Uv-Vis data for each timepoint collected during the generation of the Residence Time Distribution	43
Figure 16	Reaction conditions for aerobic oxidation of 2,2,2-trichloroethyl (*Z*)-2-(4-bromophenyl)-2-hydrazonoacetate in flow	45

Figure 17	Split test results for batch hydrazone oxidation	46
Figure 18	Flow setup for continuous processing of diazo compounds	49
Figure 19	Results from the parameter space exploration showing the effects of air and liquid flow rate, hydrazone concentration, and gas to liquid flow rate ratio on diazo yield	53
Figure 20	Residence time distribution curve	58
Figure 21	Performance of hydrazone oxidation process over 11 residence times	60
Figure 22	Semi-batch set-up and reaction scope for downstream dirhodium(II)-carbene utilization of diazo compounds	62

LIST OF SYMBOLS AND ABBREVIATIONS

C–H	Carbon–Hydrogen
Rh_2L_4	Chiral dirhodium(II) tetracarboxylate catalyst
TON	Turnover number
TOF	Turnover frequency
DOSP	(*p*-dodecylphenyl-sulfonyl)prolinato
(*p*-BrTPCP)	(4-bromophenyl)-2,2-diphenyl-cyclopropanecarboxylato
(*o*-ClTPCP)	(2-chlorophenyl)-2,2-diphenyl-cyclopropanecarboxylato
(*S*-2-Cl-5-CF_3TPCP)	(2-chloro-5-trifluoromethylphenyl)-2,2-diphenyl-cyclopropanecarboxylato
dr	Diastereomeric ratio
rr	Regioisomeric ratio
ee	Enantiomeric excess
SBA-15	Mesoporous silica
SEM	Scanning electron microscopy
TEM	Tunneling electron microscopy
DCM	Dichloromethane
NMR	Nuclear magnetic resonance spectroscopy
TGA	Thermogravimetric analysis
HMDS	Hexamethyldisilazane
ID	Internal diameter
L	Length
μ	Dynamic viscosity
ε	Void fraction

v_o	Flow velocity through the bed
d_p	Particle diameter
ρ	Fluid density
ΔP/L	Pressure drop
O–H	Oxygen–Hydrogen
WHSV	Weight hourly space velocity
u_o	Volumetric flow rate
$m_{catalyst}$	Mass of catalyst
$Cu(OAc)_2$-H_2O	Copper(II) acetate hydrate
DMAP	4-(*N,N*-dimethylamino)pyridine
HFIP	1,1,1,3,3,3-hexafluoro-2-propanol

SUMMARY

Pharmaceutical synthesis typically exhibits low process efficiency and creates large amounts of waste, as complex biologically active molecules are produced through many reaction and purification steps to yield a product with desired stereochemistry and high purity. The past few decades have seen a rise in the development of methods to achieve atom-efficient synthesis via carbon–hydrogen (C–H) functionalization. In particular, dirhodium(II) (Rh_2L_4) catalysts with donor/acceptor diazo compound precursors enable the insertion of dirhodium carbenes into C–H bonds with high regio- and stereoselectivity. However, the industrialization of this synthesis technique has been limited due to high costs of Rh_2L_4 catalysts and safety concerns associated with handling large quantities of energetic diazo compounds. This thesis aims to contribute to the resolution of these challenges by demonstrating the application of C–H functionalization to continuous processing via utilization of packed bed reactors. To this end, an immobilized Rh_2L_4 catalyst was implemented in a packed bed with a process performance commensurate to the homogeneous catalyst employed in batch, although slow catalyst deactivation was observed. Additionally, a three-phase packed bed reactor was employed for the efficient synthesis of diazo compounds via a catalytic, aerobic hydrazone oxidation. Finally, the diazo synthesis was placed upstream of a semi-batch Rh_2L_4-catalyzed reaction, exhibiting the potential utility of this method in industrially applicable synthetic transformations. The demonstrated flow to semi-batch cascade may enable industrial adoption of C–H functionalization, as the direct utilization of diazo compounds alleviates safety concerns, and low Rh_2L_4 catalyst loadings may be employed to increase TON for a lower capital cost.

CHAPTER 1. INTRODUCTION

1.1 Traditional organic synthesis and propensity for waste in the pharmaceutical industry

Synthetic organic chemistry is an invaluable tool in the transformation of simple organic molecules that are readily available from petroleum or biomass feedstocks into chemicals of higher value. These value-added chemicals may be used in many fields, from biotechnology to materials science to pharmaceuticals. When produced via traditional synthetic methods, these molecules start as hydrocarbon backbones that undergo rearrangements, condensations, or transformation by way of functional group conversions (**Figure 1**). Because the carbon–hydrogen (C–H) bonds are largely inert, they must be replaced with more reactive functional groups, such as oxygen, nitrogen, or halogen groups (among others), before the substrate may undergo the desired chemical transformation.[1-3] This approach offers great control over site selectivity, as the difference in atoms and bond strengths allows the precise targeting of certain locations on the original molecule. However, these reactive moieties are rarely present in the desired locations for chemical change, and thus must be introduced or modified prior to conversion of the substrate to the desired product, as well as removed upon completion of each respective reaction.[1] Therefore, many reaction and product isolation steps may be necessary to achieve a single target molecule, and the number of synthetic steps increases with increasing molecular complexity.

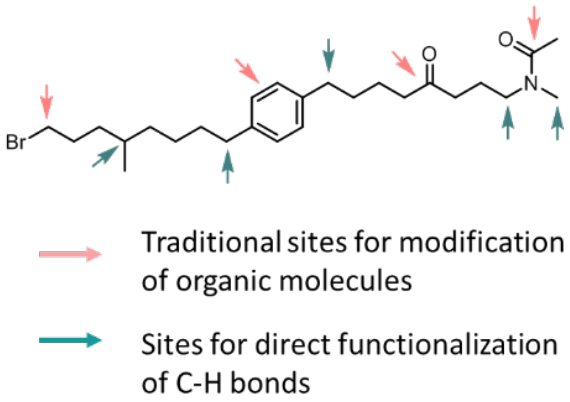

Figure 1. Traditional methods for organic synthesis rely on conversion of reactive functional groups (pink arrows), in contrast to the direct utilization of Carbon–Hydrogen (C–H) bonds (green arrows) [4]

Such processes are especially intensive in the pharmaceutical industry, where intricate biologically active compounds must be produced with exact stereochemistry and high purity. This reality is reflected in the large quantity of waste produced by the industry and can be seen in multiple sustainability metrics, such as the E factor (kg waste / kg product), atom efficiency (MW of product / sum of MW of all species), and process mass intensity (kg materials used / kg product produced).[5-7] According to Sheldon, the E factor for the pharmaceutical industry is higher than that of oil refining and the bulk and fine chemical industries combined.[6] A large contributing factor to this high waste is the huge amount of solvent used in batch reactions, solvent switching between different reaction steps, and solvent-intensive product purification via extraction, crystallization, or chromatography.[5, 8] The many necessary reaction and purification steps also leads to inevitable loss of product, which skews sustainability metrics as artificially high and incurs higher operating costs. Thus, there is not only an environmental imperative, but also a

financial incentive to implement more efficient methods to achieve total synthesis of pharmaceutical compounds.

1.2 C–H functionalization and dirhodium carbenes

The atom efficient synthesis technique of Carbon–Hydrogen (C–H) functionalization offers a paradigm shift for organic synthesis, as the utilization of C–H bonds may reduce or eliminate our reliance on traditionally-utilized functional groups. The avoidance of intermediate reaction steps would not only eliminate waste produced during total syntheses, but also avoid possible side-reactions and byproducts formed due to the presence of reactive groups in the reaction media. However, the intrinsic stability of C–H bonds necessitates the use of transition metal catalysts to carry out C–H functionalization reactions. Additionally, while the ubiquity of C–H bonds allows direct chemical transformation to take place at many different positions within an organic molecule, their prevalence also presents a selectivity dilemma: How would a reaction successfully differentiate between many energetically similar C–H bonds? Through electronics, sterics, and catalyst design, scientists have developed innovative solutions to control which C–H bond is selected during reaction. These solutions may be grouped into three general strategies: intramolecular, directed, and catalyst-controlled intermolecular reactions (**Figure 2**).[1, 3, 9-12] Intramolecular systems with two reactive sites present in the same molecule take advantage of inherent molecular orientation and spatial conformation to influence the reaction; directed reactions assert control through proximity and the utilization of directing groups that may temporarily bind to the catalyst and guide the site of reaction to a nearby C–H bond; catalyst-controlled intermolecular reactions use the size and shape of the catalytic active site to control how two reactants confront each other.[1]

Through strategic implementation of one or multiple of these strategies, scientists have developed methodologies to select between aromatic and primary, secondary, and tertiary aliphatic C–H bonds, which may undergo transformation into C–C or C–heteroatom bonds. Moreover, these methodologies have been successfully applied to total syntheses to achieve novel disconnection strategies and late-stage diversification of molecules.[9, 11, 12]

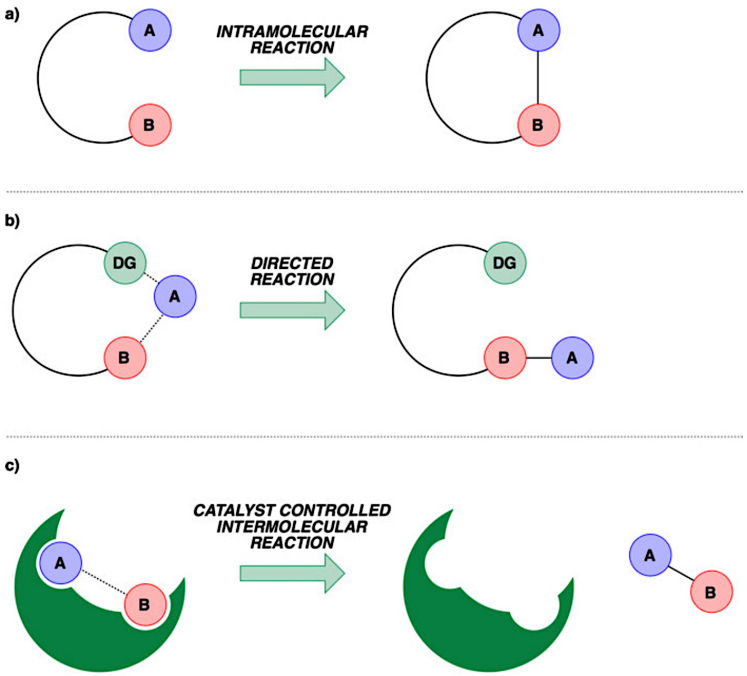

Figure 2. Illustration of general strategies to attain site selectivity in C–H functionalization reactions[13]

In particular, the use of dirhodium(II) tetracarboxylate catalysts in conjunction with donor/acceptor diazo compounds offers a novel synthetic strategy for the insertion of dirhodium carbenes into specific C–H bonds with high regio- and enantioselectivity. The catalyst structure (**Figure 3**) consists of two rhodium atoms surrounded by four chiral organic ligands (Rh_2L_4). The moieties present on these ligands may be modified to intentionally alter the electronic and steric properties of the catalyst, thereby tuning the

catalyst to selectively attack CH vs. CH_2 vs. CH_3 groups, with steric factors further dictating the location of the reaction on complex organic molecules.[14-17] Thus, dirhodium catalysts are amenable to employment in pharmaceutical processes because they are highly tunable, they are compatible with a wide range of functional groups, and their reactions typically occur at neutral pH conditions.

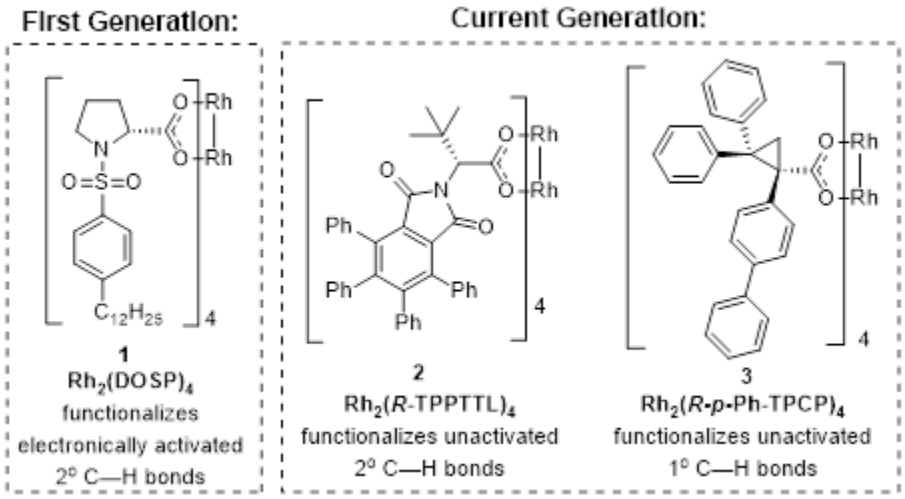

Figure 3. Select examples of dirhodium(II) tetracarboxylate catalysts.[18]

The catalytic cycle for dirhodium(II)-catalyzed intermolecular C–H insertion via a carbene transition state is shown in **Figure 4**. In this general mechanism, the diazo compound (**4**) first binds reversibly to the Rh_2L_4 catalyst (**5**). The thermodynamically-favorable evolution of nitrogen gas results in the formation of the reactive dirhodium-carbene intermediate (**7**),[19] which then inserts into a C–H bond of some substrate (**8**) to perform a desired functionalization.[20] This carbene intermediate is highly electrophilic, and thus highly reactive, which may result in a loss of selectivity; therefore, the substituents on the carbene play a critical role in modulating its reactivity. The presence of an electron-donating group on the carbene attenuates the highly electrophilic nature of this

intermediate; thus, the implementation of donor/acceptor diazo compounds is critical in imparting high selectivity to the desired C–H insertion.[18, 21, 22]

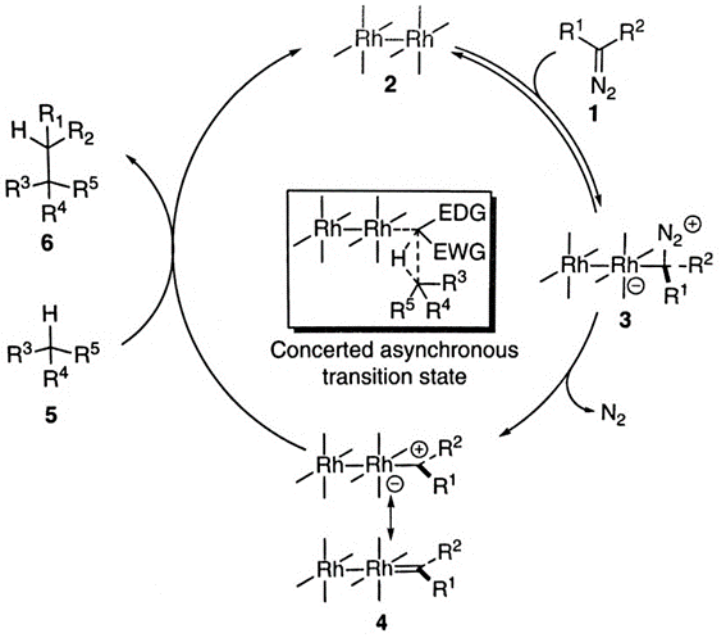

Figure 4. General mechanism for dirhodium (II)-catalyzed C–H insertion reactions with diazo compound precursors.[20]

1.3 Challenges in industrialization of dirhodium carbene-mediated C–H insertion

While there are inherent advantages to the application of C–H functionalization to the pharmaceutical industry, such as enhanced process efficiency, several challenges must be resolved before this chemistry can be implemented on an industrial scale.

One such barrier to the industrial implementation of C–H functionalization is the high cost of the noble metal and intricate synthesis of the chiral ligands that constitute the Rh_2L_4 catalysts. Rhodium is one of the rarest and most expensive transition metals,[23] making catalyst recyclability imperative to the industrial future of this chemistry. Because Rh_2L_4 catalysts are homogeneous in nature, additional purification steps are necessary to

recover the catalyst from the product stream. Furthermore, because rhodium is quite toxic, its presence in pharmaceuticals is severely limited,[23] further necessitating rigorous downstream purification. Such intensive separation processes typically result in catalyst deactivation, thus limiting the possibility of molecular catalyst recyclability. This challenge is best mitigated by maximizing the total turnover number (TON) of the dirhodium catalyst, which can be achieved via a range of techniques to prolong the catalyst lifetime, including: catalyst design and optimization, increasing the catalyst turnover frequency (TOF), or decreasing the rate of catalyst deactivation.[24, 25] Additionally, if catalyst deactivation rates are not too significant, catalyst TON can be elevated by catalyst recycle, which may be facilitated by the development of heterogeneous catalysts[26-30] that are amenable to deployment in flow reactors.

Another obstacle to widespread industrial acceptance of C–H functionalization is the safety concern associated with handling large quantities of highly energetic diazo compounds on-site. These reactive compounds are toxic and relatively unstable, with a risk of explosive behavior;[31-33] thus, storage of these compounds is undesired and just-in-time synthesis is preferred. Strategic implementation of flow chemistry easily and efficiently achieves the upstream synthesis of diazo compounds and their immediate downstream consumption. However, because the molecular Rh_2L_4 catalysts are typically employed in a homogeneous batch setup, they are not inherently amenable to flow chemistry (with the exception of a semi-batch configuration).

The work herein aims to contribute to the resolution of these previously described challenges. Through catalyst immobilization and implementation of flow chemistry via scalable reactor design, the barriers preventing industrial implementation of C–H

functionalization may be tempered, allowing this revolutionary chemistry to serve as a boon to the pharmaceutical industry.

1.4 Research Objectives

The overall goal of this study is thus to increase the practicality of C–H functionalization by demonstrating its application to continuous processing via utilization of packed bed reactors. Packed bed reactors are commonly used in industry, as they exhibit more efficient heat and mass transfer, better catalyst utilization, and higher throughput than stirred tank reactors, thus providing a savings in capital costs for reactions with faster rates.[34] The utility of packed beds was demonstrated in two reaction steps: the synthesis of the diazo compound precursor and the C–H insertion of the dirhodium carbene.

In **Chapter 2**, a strategy for heterogenizing and recycling Rh_2L_4 catalysts was demonstrated. Dirhodium(II) 1,2,2-triphenylcyclopropanecarboxylate ($Rh_2(TPCP)_4$) catalysts were immobilized on a mesoporous silica support so as to retain catalytic activity on par with the homogeneous derivative while minimizing mass transport limitations within the mesopores. The immobilized catalyst was then implemented in a microscale packed bed flow reactor and exhibited high yields and stereoselectivities for secondary C–H insertion reactions. This work was previously published in *Angewandte Chemie*.[35]

Chapter 3 seeks to address the safety concerns of diazo compounds via the development of a continuous process for the efficient synthesis and immediate consumption of diazo compounds. This system employed a milliscale packed bed to accommodate a catalytic, aerobic oxidation of hydrazone compounds into their respective diazo counterparts. The utility of this process for diazo synthesis was demonstrated by

including a semi-batch dirhodium(II) carbene reaction downstream of the packed bed, which afforded cycloaddition and activated secondary C–H insertion products with high yield and enantioselectivity. The flow to semi-batch cascade approach may have promise for industrial processes, as decreasing the loading of the homogeneous Rh_2L_4 catalyst offers a higher TON[36] than the immobilization strategy discussed in **Chapter 2**, while still accommodating the direct utilization of the energetic diazo compounds.

CHAPTER 2. IMPLEMENTATION OF IMMOBILIZED DIRHODIUM(II) CARBOXYLATE CATALYSTS FOR C–H FUNCTIONALIZATION IN A PACKED BED REACTOR

2.1 Background

2.1.1 Previous approaches to immobilize Rh_2L_4 catalysts and conduct C–H insertion in flow

The immobilization of molecular dirhodium catalysts has been reported using various strategies, from encapsulation in a polymer matrix to covalent tethering on heterogeneous supports. Davies *et al.* accomplished the immobilization of several chiral Rh_2L_4 catalysts on a crosslinked, pyridine-functionalized polystyrene resin via a cooperative effect of microencapsulation and pyridine coordination with one of the rhodium atoms.[37-39] This approach resulted in the loss of half of the catalyst's active sites, which may correspond to a lower yield or necessitate a higher catalyst loading; additionally, the noncovalent coordination may result in leaching of the catalyst. Takeda *et al.* built upon this work by covalently tethering Rh_2L_4 catalysts to a crosslinked polystyrene resin via modification of one of the catalyst's chiral ligands.[40] This polymer-immobilized catalyst was successfully implemented in a packed bed flow reactor, although some catalyst leaching was observed.[41]

Previously, the Jones group has focused on the immobilization of Rh_2L_4 catalysts, including those with (*p*-dodecylphenyl-sulfonyl)prolinato (DOSP) and (4-bromophenyl)-

2,2-diphenyl-cyclopropanecarboxylato (*p*-BrTPCP) ligands, onto a silica support. The catalyst Rh_2(*S*-DOSP)$_4$ was successfully immobilized onto a commercial silica support via a sulfonyl prolinate linker that modified one of the catalyst ligands. When employed in consecutive batch reactions, this system did not show a loss in catalytic performance over five recycles, and the catalyst was not found to leach from the support.[42] The silica-immobilized Rh_2(*S*-DOSP)$_4$ was then incorporated into a polymer/oxide composite hollow fiber as a scalable module for implementation of C–H functionalization in flow. However, the polymer employed in the fibers had low compatibility with the chlorinated solvents typically employed with Rh_2L_4 catalysts.[43] Building upon this work, various Rh_2(TPCP)$_4$ catalysts were immobilized onto a silica support, showing the broad applicability of this immobilization strategy, and implemented into a polymer hollow fiber, which was further optimized to improve solvent compatibility.[44] However, the use of the unusual polymeric hollow fiber reactor and the limited knowledge of the impact of different immobilization strategies for the target carboxylate ligands are two aspects of this prior work that could limit rapid deployment of C–H functionalization in an at-scale process.

2.1.2 Optimizing immobilization of Rh_2(TPCP)$_4$ catalysts on a mesoporous silica support (conducted by collaborators)

When considering the appropriate immobilization strategy for any chiral catalyst, one must account for the catalyst's inherent symmetry and the nature of the catalyst's binding site so as to preserve its intrinsic performance. With substituents at different positions of the ligands' aryl rings, Rh_2(TPCP)$_4$ catalysts adopt defined high-symmetry conformations that enable highly site- and stereoselective C–H functionalization reactions.

Modifying the identity and location of functional groups on the aryl rings alters the symmetry and selectivity of the $Rh_2(TPCP)_4$ catalyst;[14-17, 45] therefore, the installation of a tether for catalyst immobilization may also affect the catalyst performance. Additionally, given that Rh_2L_4-catalyzed C–H functionalization reactions are generally quite fast,[36] the immobilization of $Rh_2(TPCP)_4$ within the pores of a mesoporous silica support likely introduces mass transport limitations that may have a non-negligible effect on the overall reaction rate. To this end, a rigorous study investigating the effects of tether location and silica mesopore length on the activity of the Rh_2(*S*-*o*-ClTPCP)$_4$ catalyst was conducted by my collaborators, Dr. Chun-Jae Yoo and Dr. Wenbin Liu, which is summarized below. I then used the results from this study to inform the immobilization of a newly developed Rh_2(*S*-2-Cl-5-CF_3TPCP)$_4$ catalyst, which was employed in flow using a packed bed reactor. This study is reproduced below with permission from its original publication in *Angewandte Chemie Int. Ed*.[35]

2.1.2.1 Immobilization position

The unique C4 symmetric configuration of the Rh_2(*S*-*o*-ClTPCP)$_4$ catalyst consists of three aryl rings oriented in three different directions (as shown in **Figure 5**).[14] The C1 *o*-Cl-aryl ring **A** points towards the active rhodium site of the catalyst and constitutes the chiral reaction pocket (top view); the C2-phenyl ring **B**, which is *cis* to the *o*-Cl aryl group, points to the equatorial side of the Rh–O disk and is furthest away from the Rh center (side view); the other C2-phenyl ring **C**, which is *trans* to the *o*-Cl-aryl group, is at the "closed" rhodium face, where four phenyl rings tilt toward each other and block the second potential active rhodium site (bottom view).

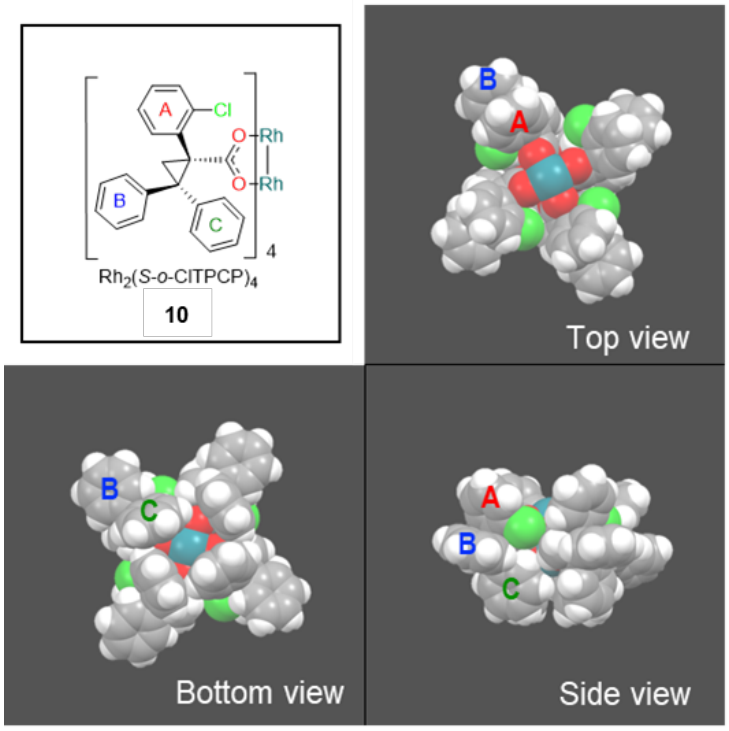

Figure 5. Chemical and crystal structures of Rh_2(*S*-*o*-ClTPCP)$_4$ catalyst (Teal: Rh, Red: O, Green: Cl, Grey: C, White: H). Aryl rings are labeled A, B, and C to show the possible locations for the introduction of a covalently bound tether to immobilize the catalyst on a heterogeneous silica support.

To determine the effect of tether location, three homogeneous Rh_2(*S*-*o*-ClTPCP)$_4$ derivatives were synthesized by placing an inert triazolepropyl trimethylsilane functionality on rings **A**, **B**, and **C**, respectively (**Figure 6A**). Additionally, three analogous heterogeneous catalysts tethered to a commercial silica support via rings **A**, **B**, and **C** were synthesized (**Figure 6B**). In this way, the potential effects of the additional tether covalently bound to the catalyst's chiral ligand and a possible steric hindrance between the catalytic active site and the silica support surface could be decoupled.

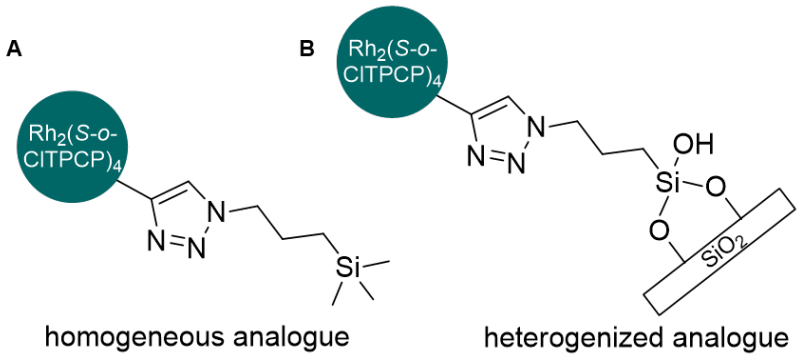

Figure 6. (A) General homogeneous Rh_2(*S*-*o*-ClTPCP)$_4$ catalyst derivative modified via inclusion of an inert triazolepropyl trimethylsilane functionality. (B) General heterogenized Rh_2(*S*-*o*-ClTPCP)$_4$ catalyst derivative modified via covalent linkage to silica support via a triazolepropyl trimethoxysilane tether.

Each of the catalyst derivatives were then subjected to a reference reaction between 4-bromopentylbenzene (**11**) and trifluoroethyl 4-bromophenyldiazoacetate (**12**). The modified catalysts all conducted the desired C–H functionalization in a stereoselective manner, as exhibited by the consistent diastereomeric ratio (dr). However, the site selectivity (regioisomeric ratio, rr) and enantiomeric excess (ee) were slightly influenced by the ligand modification (**Table 1)**. In particular, the placement of the covalent tether on ring **A** resulted in a yield, regioselectivity, and enantiomeric excess that were lower than those of the unmodified catalyst and the other derivatives for both the homogeneous and heterogeneous analogues. Thus, we may conclude that the presence of a linker at position **A** affects the active site structure and may sterically hinder the substrate's approach to the reactive carbene. Tethering the Rh_2(*S*-*o*-ClTPCP)$_4$ catalyst via rings **B** and **C** gave similar catalyst performance to the unmodified catalyst.

Table 1. The effect of tether location (A, B, or C) and catalyst nature (homogeneous, entries 2-4, or heterogeneous, entries 5-7) on Rh_2(*S*-*o*-ClTPCP)$_4$ catalyst performance.

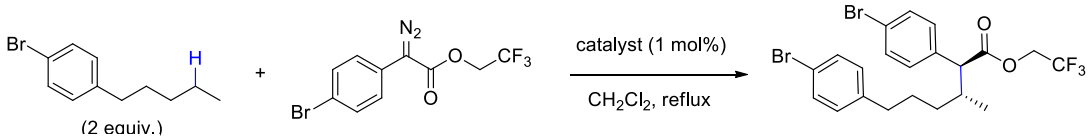

11 **12** **13**

Entry	Catalyst	Yield[a] (%)	rr (C2:Benzylic)	dr (C2)	ee (%)
1	Rh_2(*S*-*o*-ClTPCP)$_4$	87	91:9	96:4	77
2	Rh_2(*S*-*o*-ClTPCP)$_3$(tether@A)	72	88:12	95:5	72
3	Rh_2(*S*-*o*-ClTPCP)$_3$(tether@B)	83	93:7	94:6	77
4	Rh_2(*S*-*o*-ClTPCP)$_3$(tether@C)	80	91:9	95:5	77
5	Rh_2(*S*-*o*-ClTPCP)$_3$(SiO_2@A)	69	85:15	94:6	65
6	Rh_2(*S*-*o*-ClTPCP)$_3$(SiO_2@B)	83	90:10	95:5	76
7	Rh_2(*S*-*o*-ClTPCP)$_3$(SiO_2@C)	78	92:8	95:5	79

[a] Indicates isolated yield

2.1.2.2 Tuning the silica support

The high surface area and uniform pore size and structure of mesoporous silica enables the synthesis of well-defined supported catalysts; however, the presence of long straight mesopores surrounding the active rhodium sites can lead to substrate or product transport limitations, depending on the reaction conditions and the diameter and length of the mesopores. To probe the effect of mesopore length on catalyst reactivity, Rh_2(*S*-*o*-ClTPCP)$_4$ was immobilized via ring **B** on regular SBA-15 and quasi-two-dimensional, platelet SBA-15 supports. The prepared regular and platelet SBA-15 supports had similar surface area, pore volume, and pore diameter. The only distinguishable difference between each support was pore length, which was verified by SEM and TEM images (**Figure 7**). While the regular SBA-15 had a straight or slightly bent rod-shaped structure (pore length >1 μm), the platelet SBA-15 had short, straight pores (pore length < 400 nm).

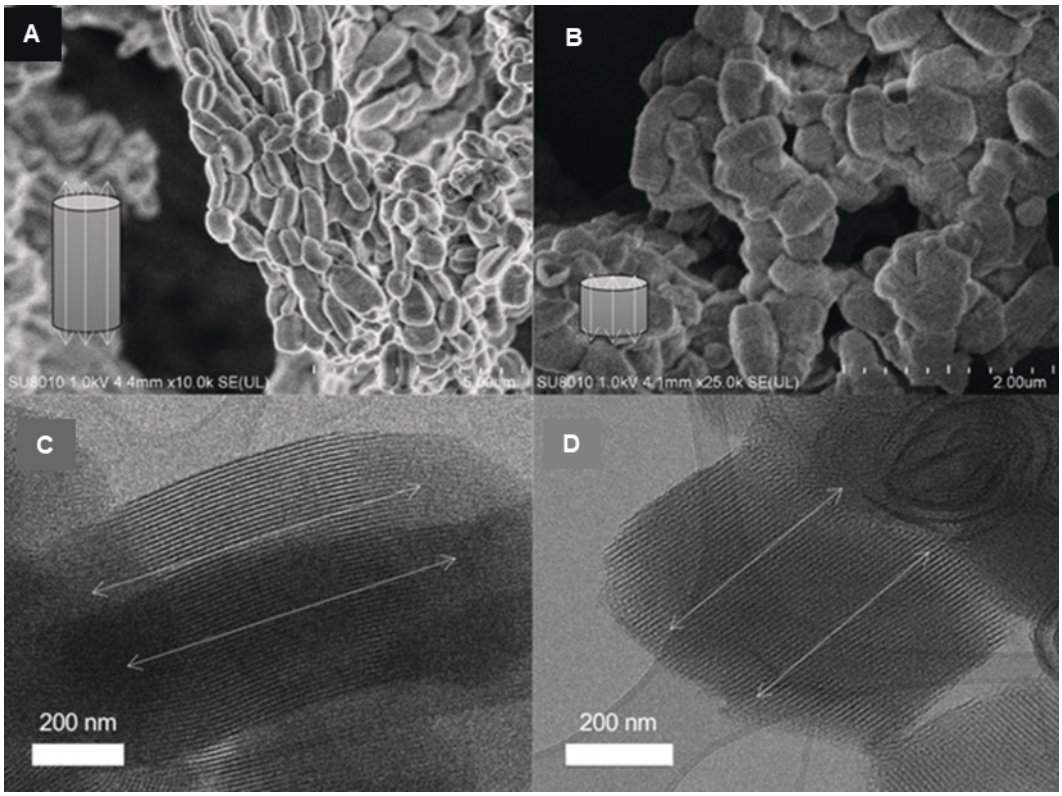

Figure 7. SEM and TEM images of (A, C) regular SBA-15 (B, D) platelet SBA-15. The white lines represent pore directions.

The two SBA-15 immobilized catalysts were subjected to a reference reaction between styrene (**15**) and trichloroethyl 4-bromophenyldiazoacetate (**14**), which was monitored via *in situ* FT-IR. The rate of the dirhodium-catalyzed cyclopropanation reaction was evaluated based on the disappearance of the peak at 2100 cm^{-1}, which corresponds to the $C{=}N_2$ stretch of the diazo compound (**Figure 8**). The reaction for each of the Rh_2(*S*-*o*-Cl-TPCP)$_4$ catalyst analogues proceeded at different rates: the homogeneous catalyst completed the reaction in 9 min, the catalyst immobilized on the quasi-2D support completed the reaction in 55 min, and the catalyst immobilized on the regular SBA-15 support completed the reaction in 125 min. The TOF of initial diazo consumption followed a similar trend. The homogenous Rh2(*S*-*o*-Cl-TPCP)4 catalyst gave a TOF that was significantly higher than that of the immobilized catalysts, and the TOF for the platelet SBA-15 immobilized catalyst was higher than that of the regular SBA-15 immobilized

catalyst, demonstrating that shortening the support channels results in an increased reaction rate.

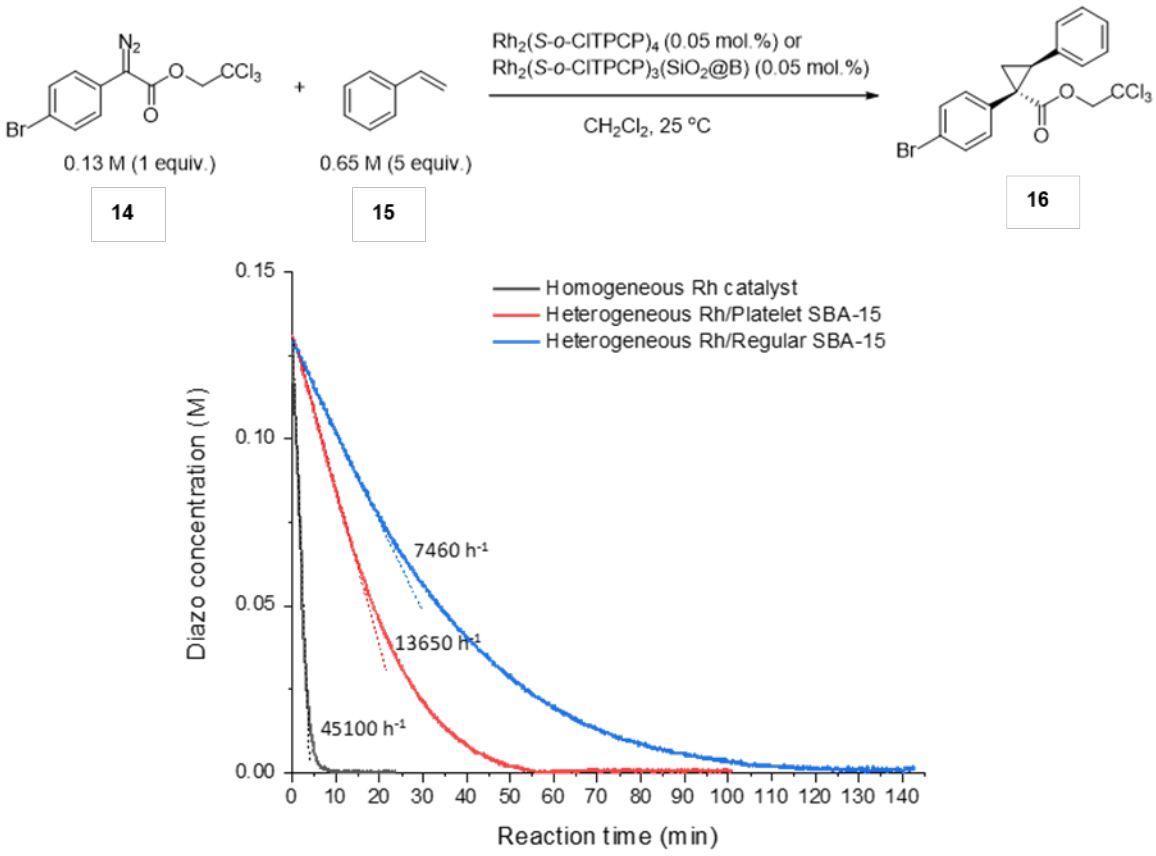

Figure 8. Effect of the length of mesopores in SBA-15 silica support on reaction time and catalyst TOF. Immobilization of the catalyst within a quasi-2D, platelet SBA-15 support mitigates some diffusional limitations of reactant to and product from the dirhodium active site, increasing catalyst TOF.

2.2 Materials and Experimental Methods

2.2.1 General Considerations

The dichloromethane (DCM) used in C–H insertion reactions was dried and degassed at reflux over activated 4 Å molecular sieves for 1 day under argon, then stored with activated 4 Å molecular sieves under argon atmosphere and was used directly. Flash

chromatography was used for product purification and performed on a Biotage® Isolera™ device. The normal phase silica columns were purchased from RediSep® and Biotage ZIP®. Diethyl ether in combination with hexanes was used in a certain gradient as the mobile phase. Analytical enantioselective chromatographs were measured on either Varian Prostar instrument or Agilent-1100 series instrument and used isopropanol/hexane as gradient. Chiral HPLC conditions were determined by obtaining separation of the racemic products using Rh_2(*R/S*-DOSP)$_4$ or Rh_2(*R/S*-2-Cl-5-BrTPCP)$_4$. HPLC retention times for each C–H insertion product are detailed in the literature.[35]

Batch C – H insertion reactions using the homogeneous Rh_2(*S*-2-Cl-5-CF_3TPCP)$_4$ catalyst were conducted by Dr. Wenbin Liu according to the literature procedure.[35]

^{1}H- and ^{13}C-NMR spectra were recorded at 400 MHz (^{13}C at 101 MHz) on a Bruker AV3 400 spectrometer. NMR spectra were run in solutions of deuterated chloroform ($CDCl_3$) with tetramethylsilane (TMS) as an internal standard (0 ppm for ^{1}H, and 0 ppm for ^{13}C) and were reported in parts per million (ppm). Abbreviations for signal multiplicity are as follow: s = singlet, d = doublet, t = triplet, q = quartet, m = multiplet, dd = doublet of doublet, etc.

Material characterization utilized the following instrumentation. IR spectra were collected on a Nicolet iS10 FT-IR spectrometer and reported in unit of cm^{-1}. Scanning electron microscopy (SEM) images were taken with a Hitachi 8230 FE-SEM. Transmission electron microscopy (TEM) images were taken with a Hitachi HT7700 TEM. Thermogravimetric analysis was conducted using a Netzsch STA-409 Luxx –

thermogravimetric analyzer – differential scanning calorimeter (TGA-DSC). Cryogenic nitrogen physisorption experiments were conducted on a Micromeritics Tristar.

The following reagents were purchased from commercial sources (Sigma-Aldrich, Alfa-Aesar, Strem Chemicals, Oakwood Chemical, and TCI America) and used directly without further purification (unless otherwise stated): hydrochloric acid (36.5-38%); Pluronic P123 (P123); ammonium fluoride (NH_4F); decane, tetraethylorthosilicate (TEOS); triphenylphosphine; methanol; copper(II) bromide; 3-chloropropyltrimethoxysilane; sodium azide; anhydrous dimethylformamide (DMF); diethyl ether; magnesium sulfate ($MgSO_4$); anhydrous toluene; triethylamine; *N,N*-diisopropylethylamine (DIPEA); Silica (SiliaFlash® P60, 40-63 μm); hexamethyldisilazane (HMDS); 1-bromo-4-ethylbenzene; 4-pentylphenyl acetate; 2,5-dibromo-3-pentylthiophene; 1-bromo-4-pentylbenzene.

The following compounds were prepared by Dr. Wenbin Liu according to literature procedures: methyl 2-(3,4-dibromophenyl)-2-diazoacetate,[46] 2,2,2-trifluoroethyl 2-(4-bromophenyl)-2-diazoacetate,[47] 2,2,2-trifluoroethyl 2-(6-chloropyridin-3-yl)-2-diazoacetate,[16] 2,2,2-trifluoroethyl2-diazo-2-(4-(trifluoromethyl)phenyl)acetate,[16] 2,2,2-trifluoroethyl 2-diazo-2-(4-nitrophenyl)acetate,[45] (E)-methyl oct-2-enoate,[35] $CuBr(PPh_3)_3$,[35] Rh_2(*S*-2-Cl-5-CF_3TPCP)$_3$(ethynyl at B).[35]

2.2.2 Synthesis of platelet SBA-15

The synthesis of platelet SBA-15 was adapted from a previously reported procedure.[48] First, 1.2 M HCl was made via dropwise addition of 8.28 mL of concentrated HCl to 21 mL of deionized (DI) water under stirring and adjusting the final volume to 84

mL with DI water. The HCl solution was added to a 1000 mL Erlenmeyer flask, along with 2.4 g of P-123 triblock copolymer. The P-123 was stirred for two hours, until it completely dissolved into solution. The solution was then heated to 35 °C and 0.027 g of NH_4F was added and stirred for another 30 minutes. Decane (13.8 g) and TEOS (6.637 g) were pre-mixed in a separate beaker and then added to the stirring HCl solution. A glass funnel was placed in the mouth of the Erlenmeyer to serve as a condenser and prevent evaporation, and this solution was left to stir at 35 °C for 20 hours. The solution was then transferred to three 50 mL Teflon-lined metal autoclaves, which were tightened with a vice. All three autoclaves were transferred to an oven (preheated to 100 °C) and left for 48 hours. To obtain the final product, the white precipitate was filtered from the autoclaves and washed with 3 L of DI water, dried at 75 °C overnight, and calcined according to the following procedure: (i) ramp to 540 °C at a rate of 2 °C/min; (ii) hold at 540 °C for 5 hours; (iii) cool to room temperature at a rate of 10 °C/min. The resulting platelet SBA-15 was characterized (**Table 2**) via cryogenic N_2-physisorption (**Figure 9**) and SEM/TEM imaging (**Figure 10**).

Table 2. Characterization of platelet SBA-15

Surface area[a]	529 m^2/g
Adsorption pore volume[a]	1.14 cm^3/g
Pore width[a]	13 nm
Pore length[b]	< 400 nm

[a] Determined via cryogenic N_2-physisorption. [b] Determined via TEM imaging.

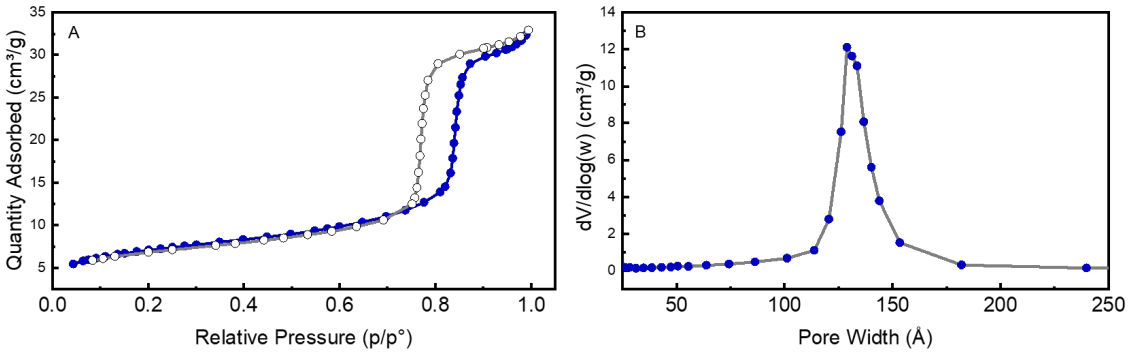

Figure 9. Adsorption and desorption isotherms and pore size distribution of platelet SBA-15 from cryogenic N_2-physisorption

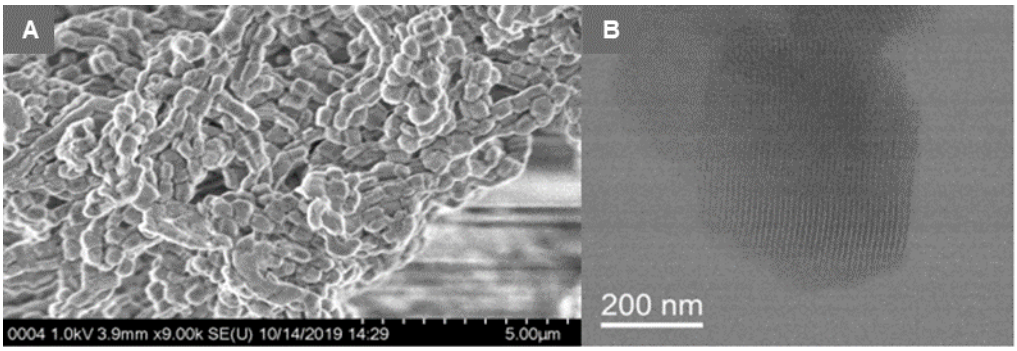

Figure 10. (A) SEM and (B) TEM (200 nm) images of platelet SBA-15

2.2.3 *Rh_2(S-2-Cl-5-CF_3TPCP)$_4$ catalyst immobilization and characterization*

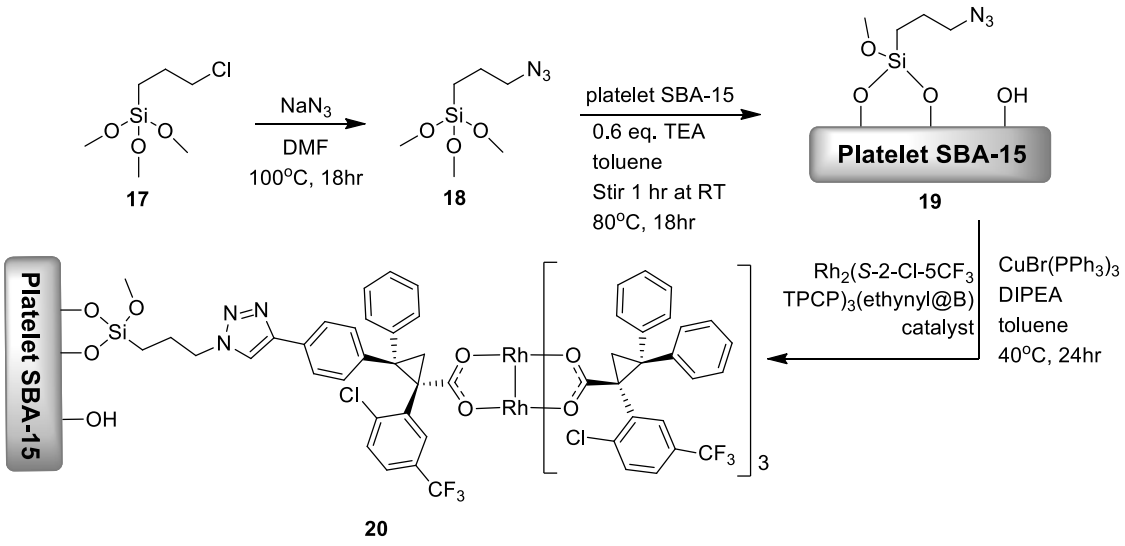

Scheme 1. Preparation of Rh_2(*S*-2-Cl-5-CF_3TPCP)$_4$ immobilized catalyst

2.2.3.1 Synthesis of 3-azidopropyltrimethoxysilane

A dry round bottom flask was charged with 3-chloropropyltrimethoxysilane (7.5 mmol), sodium azide (11 mmol), and anhydrous DMF (10 mL) under inert gas. The reaction was then stirred at 100 °C for 18 hours. The resulting 3-azidopropyltrimethylsilane was extracted with diethyl ether and DI water. The organic layer was saved and washed three additional times with DI water and once with brine. The organic layer was then dried over $MgSO_4$, filtered via gravity filtration, and subjected to rotary evaporation to remove the diethyl ether and collect the final product. NMR spectra were collected and matched with previous literature:[49] **^{1}H-NMR:** (400 MHz, $CDCl_3$) δ 3.57 (s, 9H), 3.27 (t, 2H), 1.74-1.67 (m, 2H), 0.74-0.67 (m, 2H); **^{13}C-NMR:** (101 MHz, $CDCl_3$) δ 53.86, 50.72, 22.58, 6.46.

2.2.3.2 Grafting 3-azidopropyltrimethoxysilane to platelet SBA-15 support

Previously prepared platelet SBA-15 (0.5 g) was added to a 100 mL round bottom flask, heated to 100 °C, and dried at 50 mTorr overnight. The next day, anhydrous toluene (30 mL) was added to the silica under inert gas. The solution was stirred for one hour at room temperature until it was homogeneous. The 3-azidopropyltrimethoxysilane (30.8 mg) and triethylamine (695 μL) were dissolved in 1 mL of anhydrous toluene and added to the round bottom flask. This final mixture was stirred at room temperature for one hour to allow the silane to uniformly diffuse into the pores of the SBA-15. The reaction mixture was then heated to 80 °C and stirred for 20 hours. The final grafted silica was separated from the reaction mixture via centrifugation and purified by sequentially dispersing the silica in 60 mL of toluene, hexanes, and methanol (centrifuging and decanting the solvent between each wash). The product was then dried at 70 °C for two hours and placed under 50 mTorr vacuum at room temperature overnight to remove any strongly adsorbed solvent.

The azido-grafted SBA-15 supports were then characterized by TGA to quantify the amount of silane present on the support (0.11 mmol/$g_{support}$) and IR to confirm the presence of the azido group (**Figure 11 A, B**). The presence of a small peak at 2108 cm^{-1} corresponds to the azide signature peak and demonstrates the presence of the azido group on the silica surface. Previous literature has grafted azidosilanes to silica surfaces in toluene at reflux without degradation;[50] thus, we expect the azido group to be stable during our milder grafting procedure. N_2-physisorption experiments (**Figure 11 C, D; Table 3**) shows slight decreases in pore volume and surface area compared to the bare silica support, which suggests that the azidosilanes are distributed within the pores of the SBA-15 support.

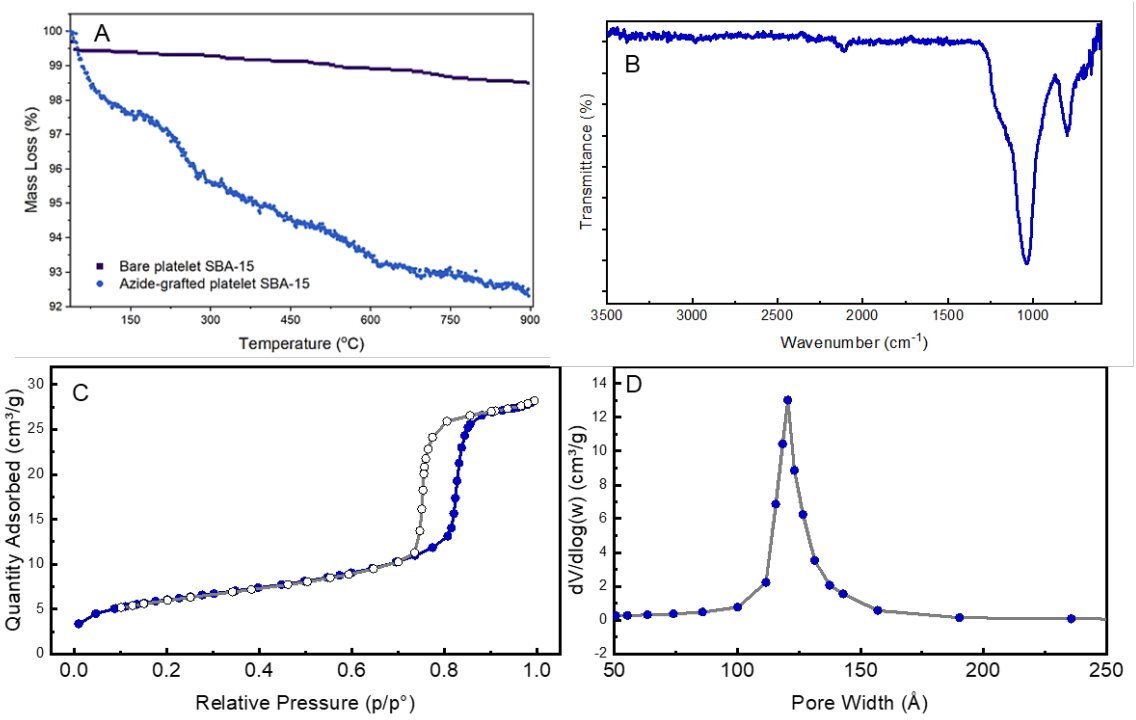

Figure 11. (A) TGA curve for azido-grafted platelet SBA-15. The mass loss corresponds to a loading of 0.11 $mmol_{silane}/g_{support}$. (B) IR curve for azido-grafted platelet SBA-15. The peak at 2108 cm^{-1} corresponds to the azide signature peak, indicating successful grafting reaction. The small size of the peak is likely due to immobilization of silane predominately within the mesopores. (C) Adsorption and desorption isotherms and (D) pore size distribution of azido-grafted platelet SBA-15 from cryogenic N_2-physisorption.

Table 3. Characterization of azido-grafted platelet SBA-15

Surface area[a]	471 m^2/g
Adsorption pore volume[a]	0.9 cm^3/g
Pore width[a]	13 nm
Azidosilane loading[b]	0.11 $mmol/g_{support}$
Yield of immobilization[c]	37%

[a] Determined via cryogenic N_2-physisorption. [b] Determined via TEM imaging. [c] Calculated based on amount of azide reacted with silica surface.

2.2.3.3 Immobilization of Rh_2(S-2-Cl-5-CF_3TPCP)$_4$ on azido-grafted platelet SBA-15 support

Previously prepared azido-grafted platelet SBA-15 was dried at 60 ºC and 50 mTorr overnight. A 100 mL round bottom flask was charged with this dry azido-SBA-15 (100 mg) and 1.5 mL of anhydrous toluene, which was stirred at room temperature for one hour to achieve a homogeneous solution. To accommodate the [3+2]alkyne-azide cycloaddition reaction to tether the catalyst to the support. The Rh_2(*S*-2-Cl-5-CF_3TPCP)$_4$ catalyst bearing a terminal ethynyl group at ring **B** was synthesized by Dr. Wenbin Liu according to literature procedure.[35] A [3+2]alkyne-azide cycloaddition reaction was then employed to tether the catalyst to the support. The ligand-exchanged catalyst (37.8 mg), CuBr(PPh)$_3$ (7.43 mg), and DIPEA (40 uL) were dissolved in 1 mL of anhydrous toluene, which was injected into the round bottom flask. The temperature was then increased to 40 ºC and the reaction progressed for 48 hrs. The silica-supported catalyst was recovered via filtration and rinsed several times with DCM and hexane. The sample was then dried overnight via lyophilization.

Insufficient quantity of sample was recovered to conduct N_2-physisorption of the Rh-immobilized platelet SBA-15 support, but the successful immobilization of the rhodium complex was confirmed with elemental analysis (catalyst loading of 0.08 $mmol_{Rh2}/g_{support}$). Additionally, because 73% of the azido groups (which were previously shown to be distributed within the mesopores) were reacted with the dirhodium complex, we can assume that the complex is distributed within the pores of the SBA-15 supports. Although some unreacted azido groups do remain on the silica support, we do not expect

them to interfere with the C–H functionalization reaction, which occurs at room temperature.

2.2.4 Hexamethyldisilazane-capped silica synthesis and characterization

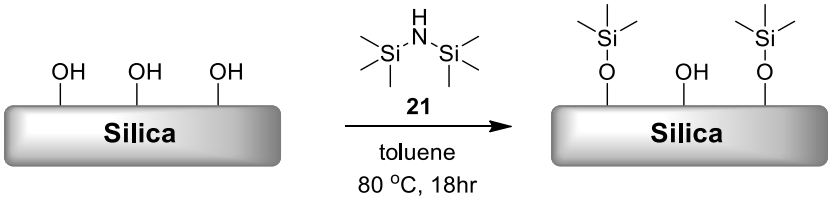

Scheme 2. Synthesis of HMDS-capped hydrophobic silica surface

Commercial silica (Siliaflash P60) (3 g) was added to a 250 mL round bottom flask, heated to 100 °C and dried at 50 mTorr overnight. Hexamethyldisilazane (HMDS) (21 mL) and anhydrous toluene (50 mL) were added to the commercial silica under inert gas. The mixture was stirred for one hour at room temperature to ensure a homogeneous solution. The reaction flask was then heated to 80 °C and allowed to react for 18 hours. The final hydrophobic silica was then collected via centrifugation and purified via redispersion in toluene several times. The success of the grafting procedure was confirmed with TGA (**Figure 12**), and the HMDS loading was found to be 0.72 mmol/g_{silica}.

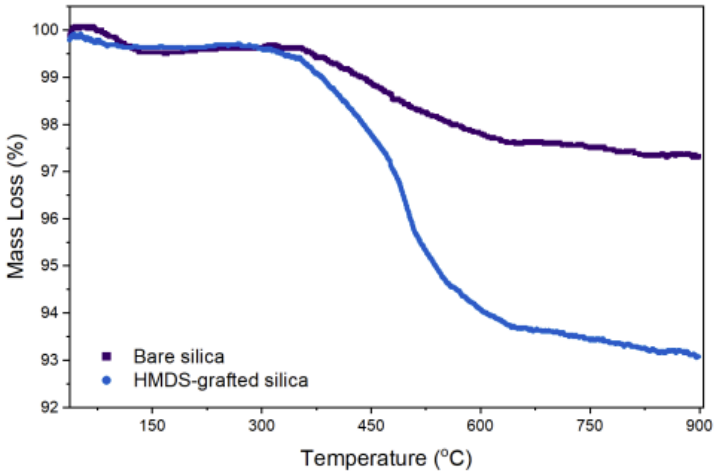

Figure 12. TGA curve for HMDS-grafted silica (loading = 0.72 mmol/g_{silica}).

2.2.5 General flow procedure for C–H insertion in a packed bed

The flow process diagram is shown in **Figure 13**. To assemble the packed bed reactor, an Omnifit glass column (ID = 3 mm, L = 25 mm) was packed with a cotton plug and a 4:1 mass ratio of HMDS-capped silica to Rh_2(*S*-2-Cl-5-CF_3TPCP)$_4$-immobilized platelet SBA-15. To pack the column, Rh_2(*S*-2-Cl-5-CF_3TPCP)$_4$-immobilized platelet SBA-15 (8.5 mg) and HMDS-capped silica (33 mg) were added to a 4 mL vial and shaken to ensure a homogeneous mixture. The silica-catalyst mixture was then added to the column in a dry state while tapping the side of the column to ensure the silica was densely packed and settled evenly throughout the column.

The packed column was then connected to a manual HPLC six-port valve (Valco) via 3 mm endpieces with 0.2 µm stainless steel frits and 16-gauge PTFE tubing. The HPLC valve consisted of a 0.5 mL sampling loop and an inlet connected to a 10 mL glass syringe fitted in a syringe pump. Diazo (0.2 mmol) and substrate (0.4 mmol) were dissolved in 0.4 mL of DCM and injected into the sampling loop. The syringe pump then pushed pure DCM

through the HPLC valve at the specified flowrate, moving the reaction mixture through the tubing and packed bed column, where the product was collected in a glass vial under Argon. Two additional mL of DCM were flushed through the column to ensure complete recovery of the reaction mixture. The C–H insertion product was isolated via flash chromatography and stereoselectivity was determined via HPLC.

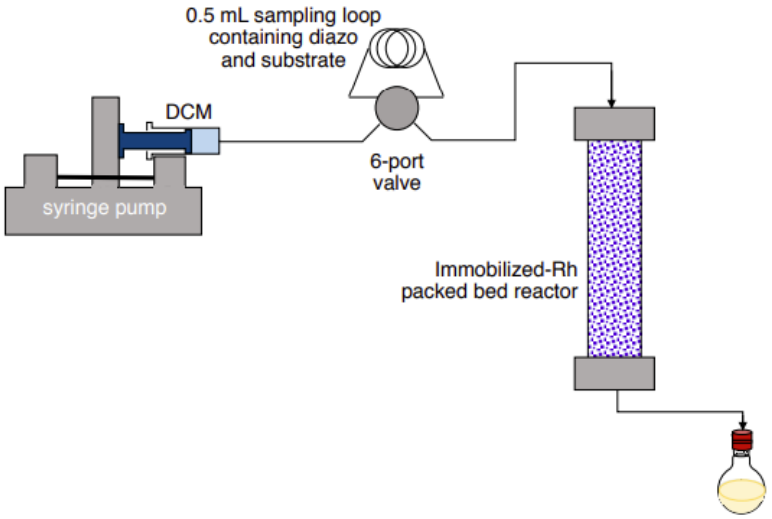

Figure 13. Flow process diagram for C–H insertion continuous process

To conduct the recyclability test, the flow set-up was constructed in the same manner; however, the packed bed was not repacked between subsequent reactions. Upon completion of the first reaction, the sampling loop was again filled with diazo (0.2 mmol) and substrate (0.4 mmol) dissolved in 0.4 mL of DCM, and the syringe pump was again allowed to push its 2 mL of DCM through the same catalyst bed. This procedure was repeated ten times sequentially.

2.3 Results and Discussion

2.3.1 Implementation of Rh_2(S-2-Cl-5-CF_3TPCP)$_4$ in a packed bed reactor

2.3.1.1 Catalyst immobilization

To ensure maximum performance of the dirhodium-carbene catalyzed C–H functionalization reaction in a packed bed, we sought to heterogenize a high performing Rh_2L_4 catalyst using an optimized immobilization procedure. To this end, the newly developed Rh_2(*S*-2-Cl-5-CF_3TPCP)$_4$ catalyst was chosen for immobilization because it offers regio- and enantioselectivity that outperforms that of other Rh_2L_4 catalysts.[35] The immobilization strategy utilized for this catalyst was determined based on the results of the previously discussed immobilization study conducted by Dr. Chun-Jae Yoo and Dr. Wenbin Liu (**Section 2.1.2**). Based on the previous result, the Rh_2(*S*-2-Cl-5-CF_3TPCP)$_4$ catalyst employed in our packed bed was immobilized via aryl ring **B** onto a platelet SBA-15 support. Although the previous result did not show a distinct difference in Rh_2(*S*-*o*-ClTPCP)$_4$ performance when immobilized via rings **B** or **C** (**Table 1**), we decided to immobilize the Rh_2(*S*-2-Cl-5-CF_3TPCP)$_4$ via ring **B**. Because ring **B**'s equatorial position is conserved in other TPCP catalyst geometries, immobilization via this ring affords access to both rhodium active sites and is therefore the optimal anchor site for all known TPCP-based dirhodium catalysts.[14-17, 45, 51, 52] Additionally, the Rh_2(*S*-2-Cl-5-CF_3TPCP)$_4$ catalyst was immobilized onto a platelet SBA-15 support to minimize mass transfer limitations within the packed bed, thus allowing for a shorter residence time to maximize catalyst performance. Details of the catalyst immobilization are discussed in **Section 2.2.3**.

2.3.1.2 Packing the reactor

While immobilization onto the platelet SBA-15 offers many boons, such as a high surface area to maximize catalyst immobilized onto the surface and low pore length to maximize catalyst TOF, the small particle size (>400 nm) offers a distinct disadvantage as well. Such a small particle would introduce enormous pressure drop across the packed bed, likely preventing any fluid flow. Thus, the immobilized catalyst was diluted with commercial silica before implementation in the packed bed. The Ergun Equation[53] may be used to estimate pressure drop along a given bed length:

$$\frac{\Delta P}{L} = \frac{150\mu(1-\varepsilon)^2 v_o}{\varepsilon^3 d_p^2} + \frac{1.75\rho(1-\varepsilon)u_o^2}{\varepsilon^3 d_p} \quad (1)$$

Where μ represents the dynamic viscosity of DCM (4.13×10^{-4} kg $m^{-1}s^{-1}$), ε is the void fraction of the packed bed (estimated as 0.37 for spherical particles), v_o is the flow velocity through the bed (m s^{-1}), d_p is the diameter of the particles in the bed packing (m), and ρ is the density of DCM (1326 kg m^{-3}). According to this calculation, diluting the platelet SBA-15 immobilized catalyst with commercial silica (SiliaFlash P60, 40-63 μm) in a 1:4 mass ratio of immobilized catalyst to silica offers nearly an 18,000× decrease in ΔP/L. Such a dramatic decrease in pressure drop allowed the successful implementation of the platelet SBA-15 immobilized catalyst into the packed bed reactor.

While the introduction of commercial silica into the packed bed mitigated pressure drop, the abundance of silanol groups on the hydrophilic silica surface resulted in the introduction of O–H insertion reactions, which competed with the desired C–H insertion and lowered the process performance. Therefore, the silanol groups were passivated with

HMDS (**Section 2.2.4**) to create a hydrophobic silica surface that would attenuate O–H insertion reactions.

2.3.1.3 Flow rate determination

To determine the optimal flow rate for the process, the performance of the immobilized catalyst implemented in the packed bed was compared to both the homogeneous catalyst and the catalyst immobilized on commercial silica in batch. As shown in **Table 4**, the flow process gave regio-, diastereo-, and enantioselectivities analogous to the batch reactions. However, the flow rate of the reaction stream did have a significant effect on the yield of the C–H insertion product. A flow rate of 0.02 mL/min was found to give a yield comparable to that of the immobilized catalyst implemented in batch (75% vs 78%, respectively).

Table 4. Effect of flow rate on catalyst performance

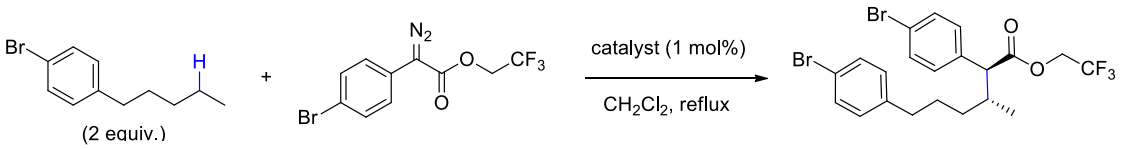

Rh_2(*S*-2-Cl-5-CF_3TPCP)$_4$ catalyst derivative	Flow Rate (mL/min)	Yield[a] (%)	rr (C2:benzylic)	dr (C2)	ee (%)
Homogeneous, unmodified	batch	82	28:1	20:1	93
Immobilized on commercial silica	batch	78	>30:1	20:1	93
Immobilized on platelet SBA-15	0.05	46	>30:1	22:1	94
Immobilized on platelet SBA-15	0.02	75	30:1	25:1	94

[a] Indicates isolated yield.

2.3.2 Process Performance

With optimized packing and flow rate, the utility of the packed bed reactor was then demonstrated with a limited substrate scope of secondary C–H insertion reactions. The performance of the packed bed reactor was compared to that of the homogeneous Rh_2(*S*-2-Cl-5-CF_3TPCP)$_4$ catalyst employed in batch, as shown in **Figure 14.** With two exceptions (**24c**, **24d**), the C–H insertion products were synthesized with high yields (75-93%), as well as regio-, stereo, and enantioselectivities (86-95% *ee*) commensurate with those obtained via the homogeneous/batch analogue (**24a-b, 24e-i**). At the pre-determined flow rate of 0.02 mL/min, substrates c and d were obtained in only trace amounts; therefore, the flow rate for these reactions was further decreased to 0.01 mL/min. Although substrates **24c** and **24d** were obtained with lower yields (32% and 25%, respectively), a relatively high enantioselectivity (82% *ee*) was maintained in both reactions. For substrate c, the low yield is presumably caused by the slower rate of diazo decomposition due to the presence of the strongly electron-withdrawing nitro group. For substrate d, the coordination between the rhodium active site and the pyridyl nitrogen (a known poison for Rh_2L_4 catalysts)[37, 54] likely lowers the catalyst's efficiency.

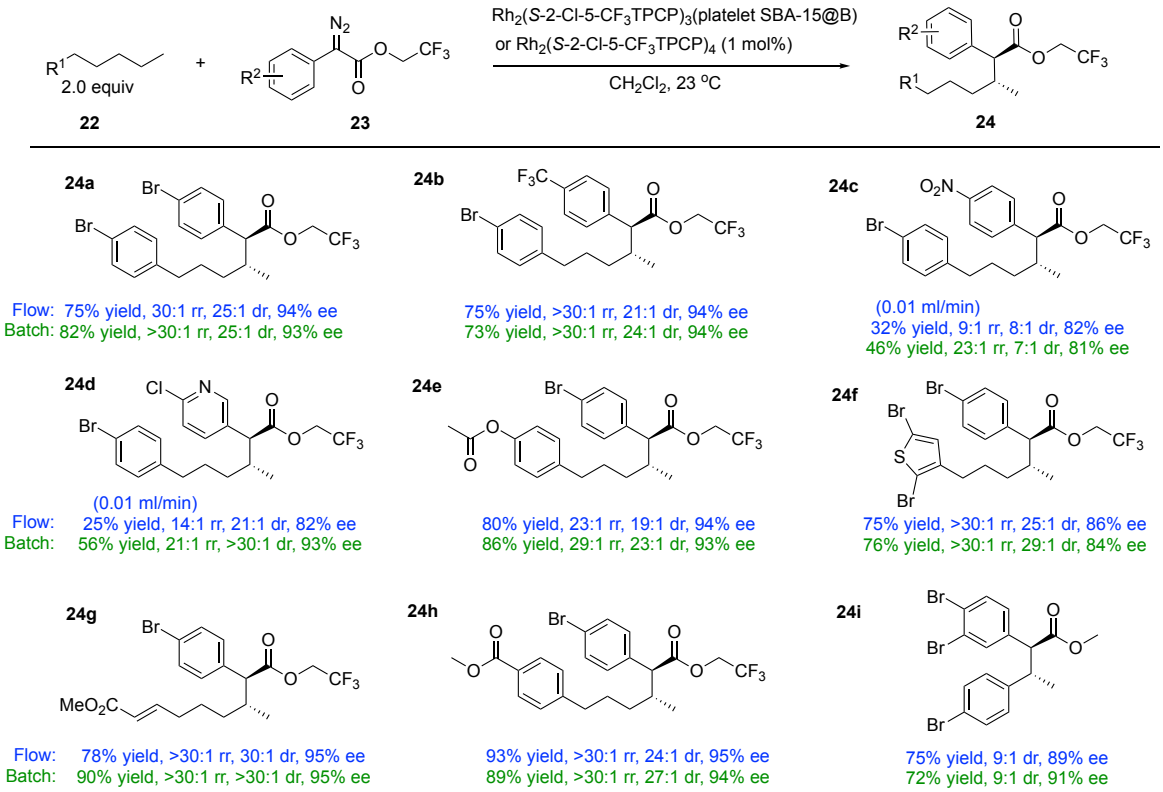

Figure 3. Substrate scope showing Rh_2(*S*-2-Cl-5-CF_3TPCP)$_4$ catalyst performance in flow (top, blue) and batch (bottom, green) reactions. The flow reactions were conducted at a flow rate of 0.02 mL/min, with the exception of substrates c and d, which were run at a flow rate of 0.01 mL/min to accommodate decreased reactivity. The given yields indicate isolated yield.

The similarity in performance between the immobilized catalyst implemented in the packed bed reactor and the homogeneous catalyst employed in batch supports our previous hypothesis that the immobilization via the equatorial ring **B** is robust and may be broadly applied to other Rh_2(TPCP)$_4$-derived catalysts. Additionally, the weight hourly space velocity (WHSV) may be calculated to quantify the productivity of the system:

$$WHSV\ (hr^{-1}) = \frac{u_o \rho_{diazo}}{m_{catalyst}} \qquad (2)$$

Where u_o is the flow rate through the bed (mL hr^{-1}), ρ_{diazo} is the density of diazo in the reaction stream (mg mL^{-1}), and $m_{catalyst}$ is the mass of catalyst in the packed bed (mg). The WHSV of our system is large (570 hr^{-1} for substrates **24a-b, 24e-i**; 285 hr^{-1} for substrates **24c,d**) compared to some other reported supported catalysts for site- and enantioselective organic reactions.[55-61] This high WHSV and the low residence time (53 s for substrates **24ab, 24e-i**; 106 s for substrates **24c,d**) show that our system has an efficient use of catalyst and may be capable of achieving high productivity to enable the scale-up of this system.

One of the advantages of our catalyst immobilization strategy is that it enables the recycling of the dirhodium catalyst. To conduct our recyclability study, the same batch of catalyst was subjected to ten consecutive reactions without repacking the column between runs. As shown in **Table 5**, the yields were consistent across recycles, with only a slight decrease from 75% to 67%, and the enantioselectivities were quite stable, decreasing only slightly from 93% to 89%. As we have previously shown,[44] the rhodium catalyst is not prone to leaching from the silica support and the slight decrease in activity can be attributed to a slow deactivation of the catalyst over time.

Table 5. Recyclability results for the immobilized Rh_2(*S*-2-Cl-5-CF_3TPCP)$_4$ catalyst

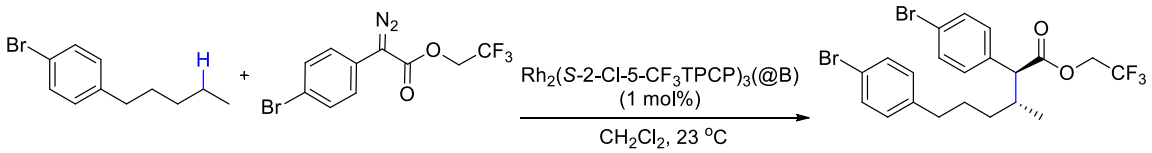

10 **11** **12**

Recycle No.	1	2	3	4	5	6	7	8	9	10
Yield[a] (%)	75	76	76	75	78	73	71	70	68	67
rr	30:1	30:1	30:1	30:1	28:1	27:1	24:1	30:1	24:1	25:1
dr	25:1	24:1	24:1	24:1	23:1	23:1	23:1	23:1	23:1	24:1
ee (%)	94	90	90	90	89	90	89	90	90	89

2.4 Conclusion

In conclusion, the previous immobilization study conducted by Dr. Wenbin Liu and Dr. Chun-Jae Yoo was applied to the heterogenization of the Rh_2(*S*-2-Cl-5-CF_3TPCP)$_4$ catalyst. The Rh_2(*S*-2-Cl-5-CF_3TPCP)$_4$ catalyst was heterogenized by immobilization via aryl ring **B** on a platelet SBA-15 support. Diluting the immobilized catalyst with hydrophobic silica enabled the implementation of the immobilized catalyst in a packed bed without a significant pressure drop. The immobilized catalyst performed secondary C–H insertion reactions with high yields and selectivities, and the packed bed performance was similar to that of the homogeneous catalyst employed in batch. Additionally, the catalytic performance was maintained over multiple recycles. Therefore, this work may demonstrate the enhanced practicality of immobilized Rh_2L_4 catalysts for implementation in an at-scale pharmaceutical process.

CHAPTER 3. DEVELOPMENT OF A CATALYTIC PROCESS FOR AEROBIC OXIDATION OF HYDRAZONE COMPOUNDS USING A THREE-PHASE PACKED BED REACTOR

3.1 Background

3.1.1 Previous approaches to synthesize diazo compounds in flow

Donor/acceptor metal carbenes derived from diazo compounds exhibit high reactivity and may undergo a wide range of cross-coupling,[62, 63] cycloaddition,[64, 65] X–H insertion (X=O, N, S, Si),[66-68] and C–H insertion reactions with high site- and enantioselectivity.[69] Despite the broad synthetic utility of donor/acceptor diazo compounds, these reagents have yet to be applied on an industrial level. Due to the energetic and potentially unstable nature of diazo compounds, safety concerns of exothermic decomposition and possible explosion hazards have led to concern over their on-site storage and large-scale synthesis.[31]

Previous work has sought to address the safety limitation of diazo compounds through flow chemistry. The on-demand synthesis of diazo reagents and their immediate consumption in downstream reactions may obviate safety concerns of handling large amounts of diazo compounds in batch reactions and on-site storage. Additionally, flow synthesis may afford access to a greater scope of diazo compounds, including less stable reagents.[70] Previous literature has achieved diazo synthesis in flow via diazo transfer using tosyl azide,[71, 72] diazotization of primary amines,[73-76] hydrazone fragmentation,[77] and base-catalyzed elimination of diazald.[78-81] However, each of these methodologies generates

stoichiometric byproducts and requires large amounts of aqueous base, which may lead to diazo decomposition or undesired reactivity causing interference with downstream reactions, thus requiring in-line separation. In contrast, hydrazone oxidation offers a milder method to generate diazo compounds and water as a benign byproduct, without requiring additional separation steps. These reactions are usually performed using stoichiometric excess of metal oxides, typically MnO_2;[70, 82-85] however, the stoichiometric generation of metal waste, especially for large-scale applications, is undesirable. Hydrazone oxidation has also been conducted in flow using polystyrene-supported *N*-iodo-*p*-toluenesulfonamide potassium salt as a stoichiometric oxidant.[86, 44, 87] However, iodide leaching interfered with the downstream C–H functionalization and the oxidant must be periodically regenerated with aqueous base, thus introducing water into the system that could potentially interfere with a downstream C–H insertion. These shortcomings may be absolved with a catalytic process for hydrazone oxidation.

3.1.2 A catalytic method for hydrazone oxidation

Recently, the Davies and Stahl groups developed a batch methodology using copper(II) acetate hydrate ($Cu(OAc)_2$-H_2O) as a pre-catalyst under aerobic conditions to oxidize a wide scope of hydrazone compounds to their corresponding diazo in high yields. They found that pyridyl bases enhanced the rate of reaction by solubilizing the Cu catalyst and that the reaction rate exhibited a first-order kinetic dependence on $Cu(OAc)_2$-H_2O concentration. According to the proposed rate mechanism, the deprotonation of the hydrazone compound is likely the rate-limiting step, with pyridine-ligand exchange and catalyst oxidation occurring so quickly that the reaction rate does not exhibit a kinetic dependence on either pyridine concentration or O_2 partial pressure.[88]

In the present study, we seek to build upon this work by developing a continuous process consisting of a three-phase flow system to accommodate the aerobic hydrazone oxidation with immediate consumption of diazo in a downstream, semi-batch reaction. We investigated the robustness of the process using homogeneous Rh_2L_4 catalysts to conduct a small scope of semi-batch carbene reactions. To accommodate the Rh_2L_4-catalyzed reactions, some challenges must be accounted for when developing the flow process. First, the Stahl and Davies groups utilized pyridine-derived base additives to accelerate the reaction rate and improve hydrazone conversion.[88] However, pyridyl groups act as poisons for Rh_2L_4 catalysts due to the strong interaction of the nitrogen atom's lone pair electrons with Lewis acidic metals,[37, 54] which may lead to lower conversion in the downstream reaction. Additionally, C–H insertion reactions have better performance in solvent sparged with inert gas;[89] this may be an issue as the effluent of our aerobic oxidation stream will be enriched with O_2. Also, the presence of water as a stoichiometric byproduct of the oxidation reaction may introduce some side reactions, notably O–H insertion, in the downstream reaction.[36] Finally, Cu catalysts can react with diazo compounds to form Cu carbenes that may undergo cross-coupling reactions for C–C bond formation.[90] Thus, if appreciable amounts of Cu leach from the column, there could be some catalytic competition that may lower the selectivity of the final product.

3.1.3 Flow processes for aerobic oxidation

Several groups have developed flow systems to accommodate various aerobic oxidation reactions.[91] Previous studies employing homogeneous catalysts for oxidation have found that the reaction rate was limited by the mass transfer of oxygen into the liquid phase, and increasing the surface area of contact between the two phases increased the

reaction rate.[92-95] Other studies that employed heterogeneous catalysts in a packed bed with a three-phase reaction found that the hydrodynamic regime has a profound effect on conversion and selectivity.[96-98] Several factors influence the hydrodynamics within a three-phase system, such as the ratio of gas to liquid flow rate, the diameter of particles within the bed, and fluid properties (e.g. surface tension or viscosity).[99] Additionally, the presence of capillary forces increases as reactor diameter decreases, which creates different flow patterns and mass transfer performance in micropacked bed reactors than those observed for industrial scale processes.[96, 100-102]

With these precedents in mind, we developed a milli-scale packed bed reactor design that would enable tuning the flow rates and surface areas of air and liquid phases to study the impact of hydrodynamics on the aerobic oxidation. We found that operating in a gas-continuous regime was important for maximizing oxidation and system performance was maintained over 11 residence times. The broad utility of this system is demonstrated by placing the hydrazone oxidation upstream of a small scope of carbene reactions. To the best of our knowledge, this report is the first to describe a catalytic, aerobic oxidation of hydrazone compounds in flow.

3.2 Materials and Experimental Methods

3.2.1 General Considerations

^{1}H-NMR experiments were recorded 700 mHz on a Bruker AV3-HD 700 spectrometer. NMR spectra were run in solutions of chloroform ($CDCl_3$) using dodecane as an internal standard. UV-Vis was performed using an Agilent Cary 60 UV-Vis Spectrophotometer. All flash column chromatography was performed on silica gel

(SiliaFlash® P60, 40-63 μm). Enantiomeric excess (ee) data were obtained on a Varian Prostar chiral HPLC Varian Prostar 210, Agilent 1100, or Agilent 1290 Infinity II instruments, eluting the purified products using a mixed solution of HPLC-grade 2-propanol (iPrOH) and *n*-hexane.

The following compounds were prepared by my collaborator, Bo Wei from the Davies group at Emory University, according to literature procedures: Rh_2(*R*-*p*-PhTPCP)$_4$,[103] Rh_2(*R*-PTAD)$_4$,[104] Rh_2(*R*-TPPTTL)$_4$,[105] 2,2,2-trichloroethyl (*Z*)-2-(4-bromophenyl)-2-hydrazonoacetate.[88]

The following chemicals were purchased from Sigma Aldrich (unless otherwise stated) and used without further purification: 4-(*N,N*-dimethylamino)pyridine (DMAP); dodecane; copper(II) acetate hydrate ($Cu(OAc)_2$-H_2O); silica gel (Sorbent Technologies, 40-75 μm); 4 Å molecular sieves (pellets, 1.6 mm diameter); 1,1,1,3,3,3-hexafluoro-2-propanol (HFIP); anhydrous cyclohexane. Styrene (≥99%, contains 4-tert-butylcatechol as stabilizer), ethynylbenzene (98%), and cyclohexa-1,4-diene (97%, contains hydroquinone as stabilizer) were purified by filtering through a column of basic alumina (aluminum oxide activated, basic, brockmann I) before use. The dichloromethane (DCM) used in each reaction was degassed using argon and dried on activated 4 Å molecular sieves overnight before use.

3.2.2 Split test

The split test was conducted similarly to a previously reported procedure.[106] To conduct each reaction, 0.25 mmol of hydrazone, 0.075 mmol of DMAP (0.3 equiv.), 50 μL of dodecane, and 3 mL of anhydrous DCM were added to a vial equipped with a magnetic

stir bar. In a separate vial, 0.025 mmol of $Cu(OAc)_2$-H_2O (0.1 equiv.) was shaken with 60 mg of silica and then added to the reaction mixture. After three minutes of reaction, one reaction mixture was filtered through a short silica plug, which was rinsed with 2 mL of DCM, into a clean vial equipped with a magnetic stir bar. The vials were left open to air and the reaction progress was monitored via ^{1}H-NMR in $CDCl_3$ using dodecane as an internal standard. Each timepoint was filtered through a syringe filter (PTFE, 0.45 μm) to prevent further reaction in the NMR solution.

3.2.3 General flow procedures

3.2.3.1 Flow column set-up

A previously reported procedure for packing a bed was adapted for our purposes.[107] First 500 mg of silica were added to a custom-built glass column (ID = 10 mm, L = 5 cm), which was gently tapped to settle the particles. Then, 10 mg of $Cu(OAc)_2$-H_2O (0.05 mmol) and 60 mg of silica were added to a vial and shaken vigorously until the mixture was homogeneous. This mixture was then added to the top of the silica plug in the column and again gently tapped until the packed bed settled. The column was then connected to 16-gauge PTFE tubing at the liquid inlet and outlet ports via 3 mm endpieces with 0.2 μm stainless steel frits and 1/8 in ID tubing at the air inlet port. The flow rate of the liquid stream was controlled via a syringe pump. The air stream was supplied by an ultra-zero air tank at 10 psig; the flow rate was controlled via a 30 sccm Air Ambient Temperature Broookings mass flow control meter and monitored via a bubble column connected to the exit stream of the reactor. The column was then employed in various flow procedures, as described below.

3.2.3.2 Pulse reaction

To conduct each pulse reaction, the syringe pump upstream of the reactor was fitted with a 10 mL syringe containing 8 mL of degassed, anhydrous DCM. The packed bed was first rinsed with 1 mL of DCM provided via the syringe pump at the specified liquid flow rate. Then, 0.5 mL of 0.3 M DMAP in DCM was then injected into the PTFE tubing and pushed through the packed bed by an additional 0.5 mL of DCM. Finally, a pulse of 0.25 mmol of hydrazone, 0.075 mmol of DMAP (0.3 equiv.), and 50 μL of dodecane were dissolved in DCM at the specified concentration (0.5 mL for 0.5 M or 1 mL for 0.25 M) and injected into the PTFE tubing. The flow reaction was then conducted at the specified air and liquid flow rates. The column was rinsed with 5 mL of DCM to ensure complete recovery of the hydrazone/diazo solution from the column into a glass vial for collection. The extent of reaction was determined via ^{1}H-NMR in $CDCl_3$ using dodecane as an internal standard.

3.2.3.3 Residence time distribution

To generate the RTD, the catalyst bed is set-up as described previously. The column is pre-wet with 1.5 mL of DCM at a flow rate of 0.1 mL/min. Then, the gas flow control meter is opened to provide ultra-zero air to the column at a flow rate of 7 mL/min for 20 minutes to ensure steady state flow is reached. Finally, the DCM is replaced with a syringe containing 5 mL of 0.25 M diazo solution. Timepoints were collected by switching the reactor effluent to a new collection vial at specified intervals. Diazo concentration in each timepoint was monitored via *ex situ* UV-Vis spectroscopy via the absorbance peak at 400 nm (**Figure 15**). The final RTD curve was generated by plotting the maximum value of

each timepoint and normalizing the resulting curve based on the maximum diazo concentration.

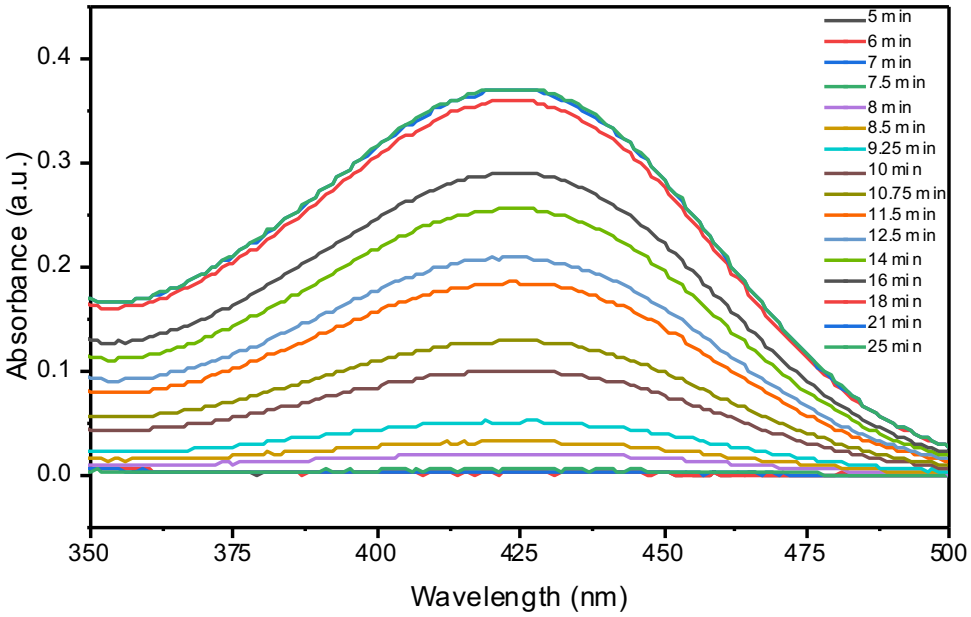

Figure 4. Raw Uv-Vis data for each timepoint collected during the generation of the Residence Time Distribution (RTD).

3.2.3.4 Time on stream

The procedure for the time on stream experiment is similar to that of the pulse reaction. The column is setup and rinsed with degassed, anhydrous DCM and a 0.3 M DMAP solution as described previously. After the pre-rinse, a 10 mL syringe containing 2 mmol of hydrazone, 0.6 mmol of DMAP (0.3 equiv.), and 400 µL of dodecane dissolved in 8 mL of DCM was placed in the syringe pump. The reaction was carried out using a liquid flow rate of 0.1 mL/min and air flow rate of 7 mL/min. Timepoints were taken by switching the reactor's exit tubing to a new vial every ten minutes. Hydrazone conversion,

diazo yield, and the concentration of diazo and DMAP eluting from the column were calculated via ^{1}H-NMR in $CDCl_3$ using dodecane as an internal standard. The elution concentration of the diazo compound was confirmed via integration of the previously generated RTD curve. The concentration of Cu in the reactor effluent was determined using ICP-OES analysis conducted by Galbraith Laboratories.

3.2.3.5 General semi-batch procedure

To conduct each semi-batch reaction, a 50 mL round bottom flask was equipped with a magnetic stir bar and flame dried. Activated 4 Å molecular sieves (4 g; dried at 200 °C and 10 mTorr overnight) were added to the flask, which was fitted with a septum and back filled with N_2. Additional care was taken to prevent introduction of water into this reaction by further drying anhydrous, degassed DCM on activated 4 Å molecular sieves overnight. (For the cyclohexane reaction, the 5 mL of cyclohexane employed as the substrate was also degassed and dried on activated 4 Å molecular sieves overnight.) The appropriate dirhodium catalyst and substrate were each dissolved in 1 mL of this dry, degassed DCM and injected into the round-bottom flask, along with an additional 3 mL of DCM. This reaction mixture was stirred for ten minutes to ensure a homogeneous solution. The flow reaction was set up using the previously described pulse procedure, with the reactor effluent connected to the septum of the round bottom flask. The semi-batch reaction solution was sparged with N_2 to minimize deleterious effects of dissolved O_2 in the reactor effluent on dirhodium catalyst performance.

3.3 Results and Discussion

3.3.1 Probing reaction conditions in batch

To adapt the copper-catalyzed aerobic oxidation of hydrazone compounds to a flow system, we focused on the oxidation of 2,2,2-trichloroethyl (*Z*)-2-(4-bromophenyl)-2-hydrazonoacetate **25** to 2,2,2-trichloroethyl 2-(4-bromophenyl)-2-diazoacetate **26** (**Figure 16**). This was chosen as a model substrate because the diazo **2** has been demonstrated to be a robust reactant in various C–H insertion reactions, exhibiting excellent reactivities and selectivities.[47] We utilized 4-(*N,N*-dimethylamino)pyridine (DMAP) as a basic additive because its increased basicity over pyridine offers a faster reaction rate,[88] which could lower the required residence time to achieve maximum conversion in a flow system. Dichloromethane (DCM) was used as the reaction solvent and silica was used as an additive in the packed bed, along with the $Cu(OAc)_2$-H_2O precatalyst.

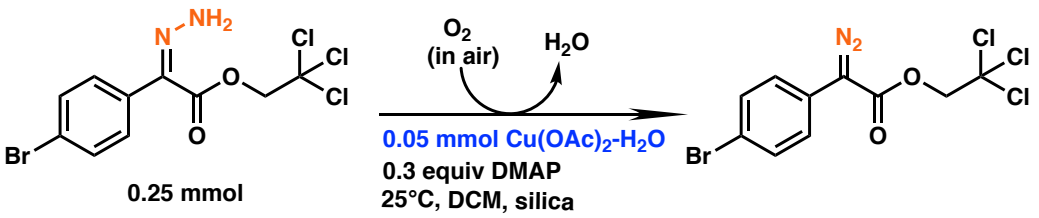

Figure 16. Reaction conditions for aerobic oxidation of 2,2,2-trichloroethyl (*Z*)-2-(4-bromophenyl)-2-hydrazonoacetate in flow

Before implementing the hydrazone oxidation reaction in flow, the $Cu(OAc)_2$-H_2O precatalyst was probed in batch conditions to give insight into the homogeneous or heterogeneous nature of the catalyst via a split test (**Figure 17**). To conduct the split test, two reactions were set up using the same conditions; however, one reaction was filtered

through a short silica plug after 3 minutes, whereas the other was left undisturbed. Upon filtration of the reaction media, reaction progress was arrested, as the Cu was visibly retained in the silica plug and hydrazone conversion remained at 66%. In contrast, the unfiltered sample reached complete conversion of hydrazone in less than ten minutes.

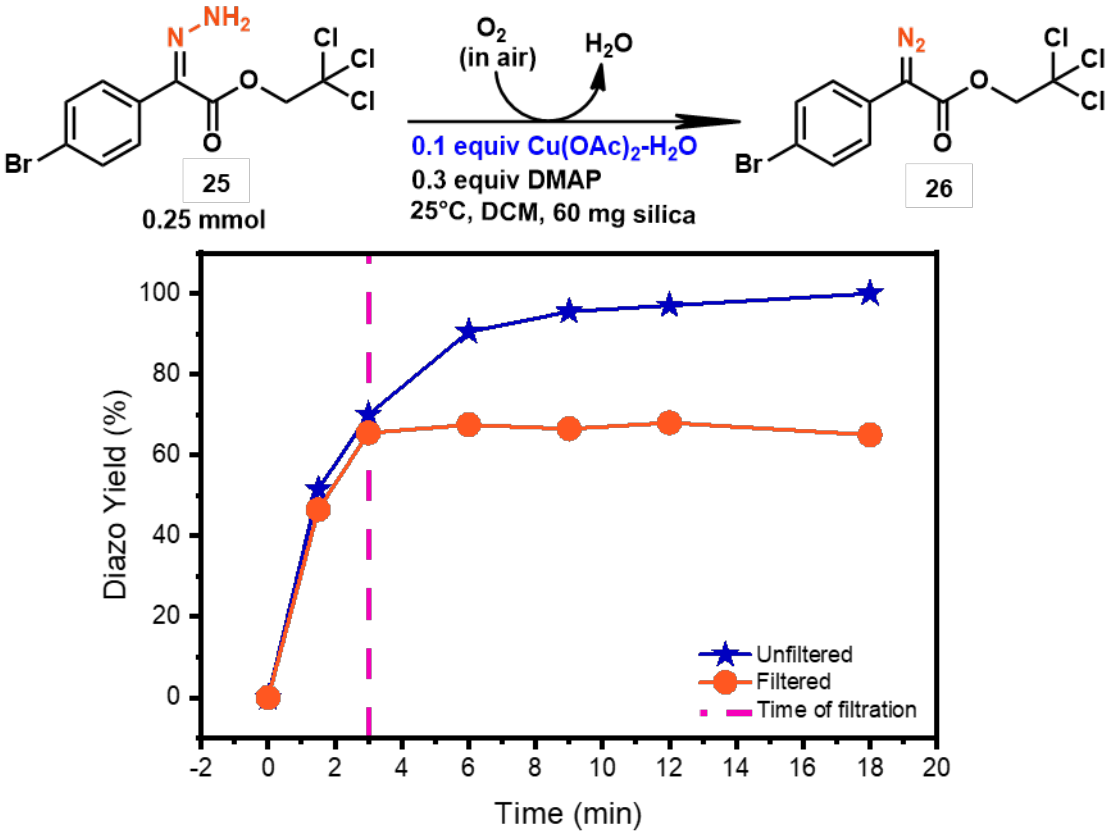

Figure 5. Split test results for batch hydrazone oxidation. The dashed line indicates time of filtration (3 minutes) through a short silica plug for the filtered sample. Diazo yield was calculated via quantitative NMR using dodecane as an internal standard.

According to the previous batch study, the $Cu(OAc)_2$-H_2O precatalyst exhibited low solubility in DCM, necessitating the inclusion of organic bases to solubilize the Cu catalyst and achieve efficient catalysis.[88] Thus, the retention of Cu species in the silica plug may be due to low solubility in DCM or polar interaction with the silanol surface. Previous

literature has shown that Cu(II) salts sorb to polar support materials in various solvents with low leaching.[108-110] Additionally, a computational study by Musaev and Liebeskind demonstrated that Cu carboxylates coordinate strongly with thiolate sulfur atoms, and this coordination is energetically favorable.[111] Thus, it is possible that a silica-sorbed Cu structure acts as a precatalyst, and DMAP-solubilized Cu is the active catalyst, and the low solubility and partitioning near the silica surface retained the active species in the column for extended periods of time.

The reversible sorption of the Cu catalyst to the silica surface would combine the effects of homogeneous and heterogeneous catalysts, namely fast reaction times and facile catalyst isolation, and support the feasibility of its implementation in a flow condition using a silica packed bed. Previous studies have implemented "catch and release" catalysts in flow reactors using strategies such as reverse-flow adsorption or release/capture columns in series.[112] In our reaction setup (explained in more detail in **Figure 18**), the $Cu(OAc)_2$-H_2O pre-catalyst is mixed with an excess of silica and placed over a silica plug, which acts as a reservoir to capture the solubilized copper catalyst from the reaction stream. This study does not utilize two separate capture/release columns with a reversible flow path; however, future studies investigating the implementation of this chemistry in a larger scale process may find this type of setup useful.

3.3.2 Optimizing the flow procedure

The flow setup for our process accommodates three-phases in a glass column, as shown in **Figure 18**. The milliscale reactor has a radius of 5 mm and bed length of 5 cm. A syringe pump containing hydrazone and DMAP dissolved in DCM pushes the liquid

phase into the top of the glass column. The oxygen is supplied via an ultra-zero air cylinder, which is within the safe flammability limits for DCM[91] and avoids introduction of additional water into the system, which could introduce O–H insertion side reactions. The flow rate of air into the column is controlled by a gas flow control meter. The headspace of the column is packed with glass wool to facilitate mixing between the co-current gas and liquid streams before the fluid phase enters the solid $Cu(OAc)_2$-H_2O/silica packed bed. The catalyst bed contains 0.05 mmol of $Cu(OAc)_2$-H_2O mixed with 60 mg of silica atop 500 mg of silica, which is supported by a glass frit. To optimize the flow procedure, we utilized "pulse" experiments as a quick diagnostic tool to evaluate process performance at various conditions. For each pulse, 0.25 mmol of hydrazone at a specific concentration was introduced into a sampling loop of tubing, which was then pushed through the column using DCM in the syringe pump. More details about the flow setup and pulse experiments are described in **Section 3.2**.

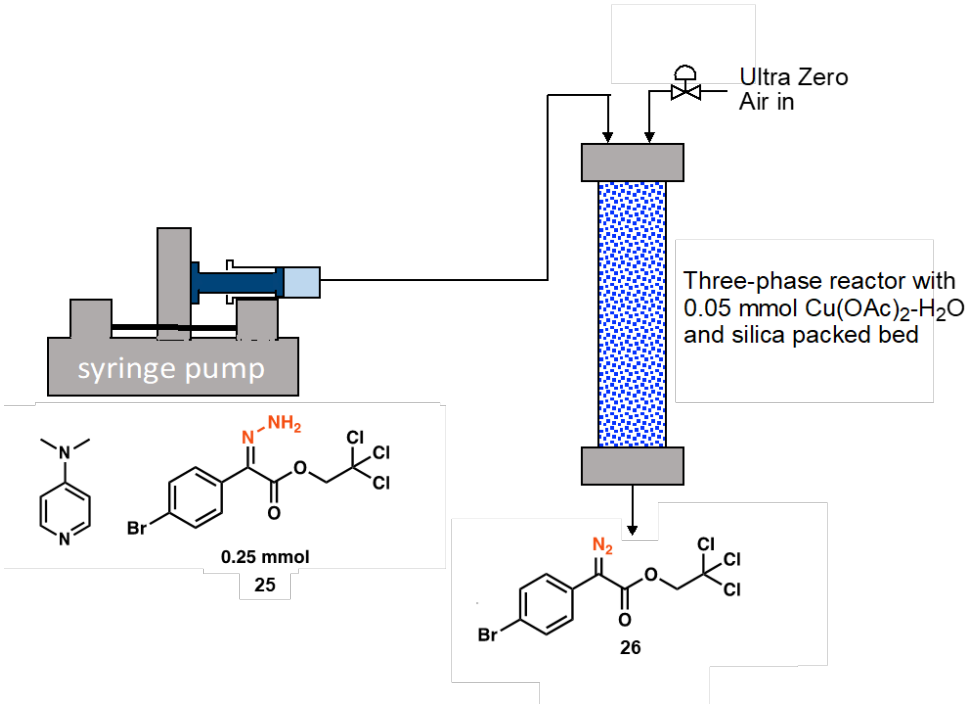

Figure 18. Flow setup for continuous processing of diazo compounds. The hydrazone and DMAP solution is introduced to the top of the column via a syringe pump, while the ultra-zero air flow rate is controlled using a mass flow controller. The co-current downflow of air and liquid enters into the packed bed of $Cu(OAc)_2$-H_2O pre-catalyst and silica, and the resulting diazo compound elutes from the column.

In determining a flow procedure, we first examined the role of DMAP in the reaction stream. Because DMAP poisons Rh_2L_4 catalysts,[54] we wanted to investigate the possibility of maximizing diazo yield while minimizing DMAP concentration in the reaction stream. We found that rinsing the column with 0.5 mL of a 0.3 M DMAP solution before introducing the hydrazone/DMAP stream increased diazo yield, while allowing a reduction in the amount of DMAP included in the reaction stream (**Table 6**). In all cases with the DMAP pre-rinse, the yield of diazo was higher (29-56%) than with a pre-rinse consisting only of solvent (19%). However, the inclusion of DMAP in stoichiometric excess of Cu in the reaction stream was necessary to regenerate the active catalyst and maintain diazo yield. Decreasing the amount of DMAP in the inlet stream from 0.6 to 0.3

equivalents to hydrazone did not show a reduction in yield, but further decreasing DMAP from 0.3 to 0.1 equivalents resulted in a significant decrease in yield, from 55% to 29%. Therefore, moving forward with optimizing the flow process conditions, we employed a prewash of 0.5 mL of 0.3 M solution of DMAP in DCM and included 0.3 equivalents of DMAP with the hydrazone stream to maintain a high diazo yield while minimizing the possible poison for downstream Rh_2L_4-catalyzed reactions.

Table 6. Effect of DMAP on reaction performance (L=1 mL/min, G=17.5 mL/min, C=0.5 M)

Entry	Pre-wash	DMAP equivalents in Pulse[a]	Diazo Yield[b] (%)
1	DCM only	0.6	19
2	0.3 M DMAP solution	0.6	56
3	0.3 M DMAP solution	0.3	55
4	0.3 M DMAP solution	0.1	29

[a] Equivalents in reference to the 0.25 mmol of hydrazone in the pulse. [b] Diazo yield was calculated via quantitative nuclear magnetic resonance (NMR) spectroscopy using dodecane as an internal standard.

Next in optimizing flow conditions, we chose to evaluate the importance of three variables in influencing diazo yield: air and liquid flow rates and hydrazone concentration. High and low values of each variable were chosen, as shown in **Table 7**, to explore a parameter space and determine the relative effect of each variable on the process performance. Simultaneously varying these parameters in a body-centered design allowed us to efficiently investigate how each variable influenced the others, along with diazo yield. Several studies have utilized this approach to successfully optimize flow processes, especially for industrial and pharmaceutical applications.[113-116]

In our case, specific boundary values for each variable were determined based on practical limitations of the design space. The minimum air flow rate (G) was chosen as 7

mL/min based on the lower range of the gas flow control meter; the maximum air flow rate was chosen as 17.5 mL/min because a higher G would have dried the packed bed, resulting in incomplete catalyst utilization due to reduced catalyst wetting.[117] The boundary values for the liquid flow rate (L) were chosen so as to traverse different hydrodynamics regimes based on the given air flow rates. The minimum hydrazone concentration (C) value was chosen to be 0.25 M because the tubing going into the reactor could accommodate a maximum volume of 1 mL of sample; the high concentration value was chosen as 0.5 M because increasing the hydrazone concentration past that point led to limited solubility. Additionally, the midpoint of the parameter space (G = 12.25 mL/min, L = 0.625 mL/min, C = 0.375 M) was performed three times to ensure the repeatability of the flow process. The midpoint results showed a diazo yield of 69 ± 3%. The low standard deviation indicates that the process is repeatable.

Table 7. Values for variables of interest in parameter space exploration

Process Variable	High/Low	Boundary value
Air Flow Rate (mL/min)	High	17.5
	Low	7
Liquid Flow Rate (mL/min)	High	1
	Low	0.25
Hydrazone Concentration (M)	High	0.5
	Low	0.25

The results of the parameter space exploration are shown graphically in **Figure 19**. **Figure 19A** shows the effect of liquid flow rate on diazo yield; **Figure 19B** shows the effect of air flow rate; and **Figure 19C** shows the effect of hydrazone concentration. In each graph, each data series corresponds to a consistent set of flow conditions in regard to the other two variables.

According to these results, liquid flow rate is the most influential variable, as decreasing liquid flow rate from 1 mL/min to 0.25 mL/min resulted in a substantial increase in diazo yield in each instance (**Figure 19A**). This observed increase is likely because decreasing liquid flow rate increases the residence time of hydrazone in the catalyst packed bed, allowing more time for the oxidation reaction to occur. The most dramatic increases in yield were observed at the lower gas flow rate (G = 7 mL/min). At these flow rates, the yield for C = 0.25 M condition increased from 31% at L = 1 mL/min to 81% at 0.25 mL/min; for the C = 0.5 M condition, the yield increased from 48% at 1 mL/min to 87% at 0.25 mL/min. This observation is likely because lowering the liquid flow rate at the low air flow rate also improved external mass transfer of O_2 into the liquid phase in addition to increasing the residence time.

Increasing the air flow rate from 7 mL/min to 17.5 mL/min had a negligible to moderate effect on diazo yield at low liquid flow rates (**Figure 19B**). However, the effect of air flow rate became more pronounced at high liquid flow rates, again likely due to increased external mass transfer of O_2 into the liquid phase. The most significant effect corresponds to conditions of L = 1 mL/min and C = 0.25 M, where diazo yield increased from 31% at an air flow rate of 7 mL/min to 57% at 17.5 mL/min. The interplay of air and

liquid flow rates was explored by investigating the ratio of gas to liquid flow rate (G:L) on diazo yield, which is pictured in **Figure 19D** and discussed in more detail below.

Finally, varying the hydrazone concentration (**Figure 19C**) exhibits a negligible effect on diazo yield, with the exception of the conditions at G = 7 mL/min and L = 1 mL/min. At these flow rates, diazo yield increases from 31% at C = 0.25 M to 48% at C = 0.5 M. The increased influence of concentration at these flow conditions is possibly because the short residence time (due to the high liquid flow rate) and low O_2 mass transfer (due to the low air flow rate) result in kinetic limitations that are partially alleviated by doubling the concentration.

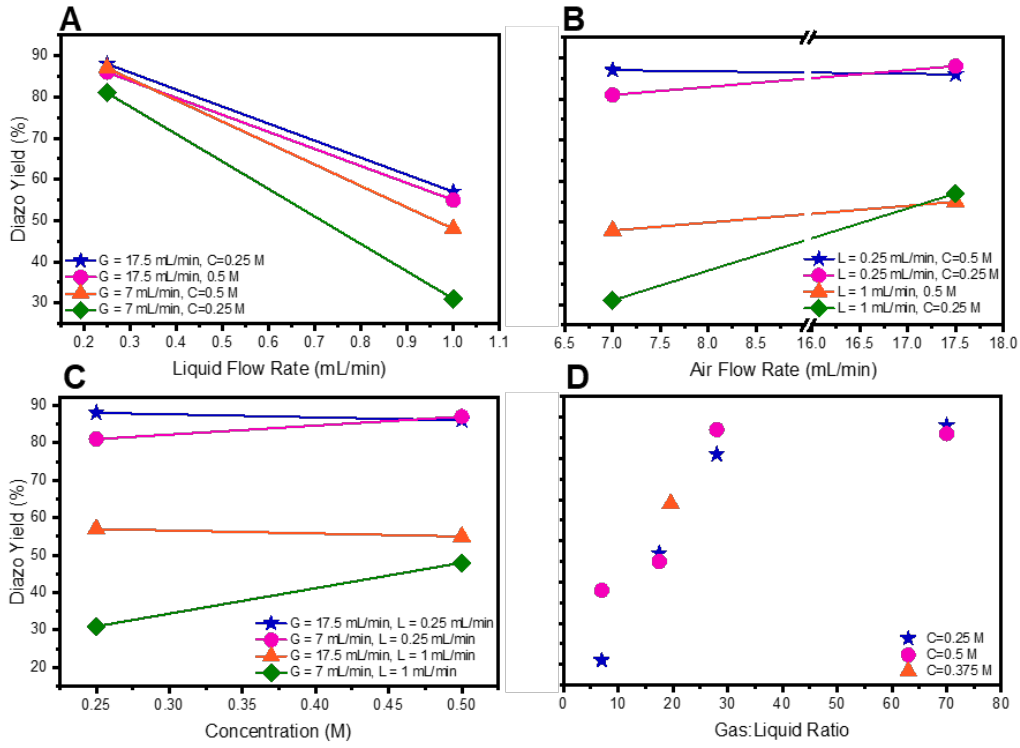

Figure 6. Results from the parameter space exploration showing the effects of air and liquid flow rate, hydrazone concentration, and gas to liquid flow rate (G:L) ratio on diazo yield. Each data series represents a consistent set of two variables to examine the influence of changing one variable (presented on the x-axis) on diazo yield. Diazo yield was

calculated via quantitative NMR using dodecane as an internal standard. (A) Effect of liquid flow rate. (B) Effect of air flow rate. (C) Effect of concentration. (D) Effect of the ratio of gas to liquid flow rate (G:L), or hydrodynamics, on diazo yield.

Figure 19D shows the ratio of gas to liquid flow rate (G:L) and the effect of this ratio on diazo yield, showing that increasing G:L results in an increase in yield at lower ratios (at or below 19.6), which plateaus at 88% for higher ratios (at or above 28). Qualifying the hydrodynamic regime within the packed bed at each of these points helps to explain this trend. Studies on micropacked bed reactors have shown that different hydrodynamic regimes exist at small scale compared to industrial scale packed bed reactors.[100, 102] Thus, due to the small scale of our reactor, we looked to the flow regime maps published by Gavriilidis *et. al.* to determine the hydrodynamics within our system. Although our reactor is slightly larger in scale than that utilized by Gavriilidis in their study, the low Re (0.0034-0.034), Bo (1.19×10^{-4}), and Ca (3.22×10^{-8} to 3.22×10^{-7}) numbers corresponding to our conditions are of a similar magnitude as the Gavriilidis system.[96] Additionally, these low values show the prevalence of capillary forces and laminar flow in our system, making a comparison to the hydrodynamics of microscale more appropriate than to industrial scale.

Table 8 lists the hydrodynamics regimes of each G:L ratio listed in **Figure 19D**. At a G:L of 7, the liquid stream dominates the continuous phase with some gas slugs interspersed;[96] therefore, the low interfacial area between the gas and liquid phases at these flow conditions corresponds to the low oxidative yield. At G:L of 17 and 19.6, a segregated flow regime is present, whereby gas and liquid phases share a relatively even volume of the packed bed, corresponding to a thick liquid film with more gas phase interspersed.[96] This results in a higher surface area of contact between the gas and liquid phases, offering

greater mass transfer of oxygen into the reaction phase, resulting in higher yield of diazo in this regime. A G:L of 28 is at the transition point from segregated to gas-continuous flow. Above this point (at G:L = 70), there is no further increase in diazo yield. The gas-continuous flow regime consists of a continuous gas phase with a thin liquid film distributed over the solid particles in the packed bed.[96] The decrease in liquid film thickness results in a higher interfacial area between the liquid and air phases, affording a further increase in mass transfer of oxygen into the liquid phase and resulting in the highest oxidative yield observed at these conditions of 88%.

Table 8. Hydrodynamic regimes encountered at different air and liquid flow rates

Air Flow Rate (mL/min)	Liquid Flow Rate (mL/min)	G:L	Predicted Flow Regime[96]	Analogous to (in macroscale)
7	1	7	Liquid-dominated slug	Pulse
17.5	1	17.5	Segregated	Trickle (thick liquid film)
12.25	0.625	19.6	Segregated	Trickle (thick liquid film)
7	0.25	28	Segregated to gas-continuous flow transition	Trickle (intermediate liquid film)
17.5	0.25	70	Gas-continuous (fully wetted)	Trickle (thin film / rivulet)
7	0.1	70	Gas-continuous (fully wetted)	Trickle (thin film / rivulet)

3.3.3 Characterization and packed bed performance

We then used the results from the parameter exploration to determine our optimized flow conditions. The optimized flow rates were achieved by lowering the liquid flow rate to increase the residence time, while maintaining a high G:L so as to remain in the gas-continuous flow regime. A liquid flow rate of 0.1 mL/min and air flow rate of 7 mL/min achieved these requirements. Another pulse study using these conditions and a hydrazone concentration of 0.5 M confirmed nearly complete conversion of hydrazone compound (99%) with a 93% yield of diazo compound. Repeating this experiment using the same flow rates and a concentration of 0.25 M gave a similar result (99% conversion and 94% yield). These results correspond well with the literature result from the previous Stahl and Davies work in batch.[88] **Figure 20** shows a residence time distribution (RTD) at these optimized air and liquid flow rates, which was generated using a step impulse of 0.25 M diazo solution at time $t = 0$. The residence time, τ, was calculated to be 7.85 min based on the catalyst bed dimensions and flow rate of the liquid stream. The following equations[34] were used to fit an nCSTR model to the step impulse timepoints:

$$\Theta = {}^{t}/_{\tau} \tag{3}$$

$$E(\theta) = \frac{C_n}{C_o} = \frac{n^n \theta^{n-1}}{(n-1)!} e^{-n\theta} \tag{4}$$

$$F(\theta) = \int_0^{\theta} E(\theta)\, dt \tag{5}$$

To fit the nCSTR model to the step impulse data, the sum of squared error of **Equation 5** was minimized relative to the data by iterating through separate values of n

(number of CSTRs). According to this fit, the flow eluting from our column is simulated as six CSTRs in series. An n below twenty CSTRs indicates deviation from ideal plug flow behavior. In this case, nonideal behavior is likely caused by channeling in the packed bed, which is common in three-phase operations.[99] Additionally, the generated F curve did not align with the plotted step impulse data, likely due to adsorption of the diazo compound to the silica in the packed bed, which delays the elution of diazo from the column. Shifting the fit curve by 0.3 residence times generates an excellent fit, as shown in **Figure 20**. Insight into the adsorption behavior can be gleaned from the time delay of 0.3 residence times. Within this time frame, according to the given solution concentration and flow rate, 0.06 mmol of diazo would be sorbed to the 560 mg of silica (surface area of 500 m^2/g) present in the column, yielding sorption behavior of 0.1 mmol diazo / g silica, or 2.1e-4 mmol diazo / m^2 silica.

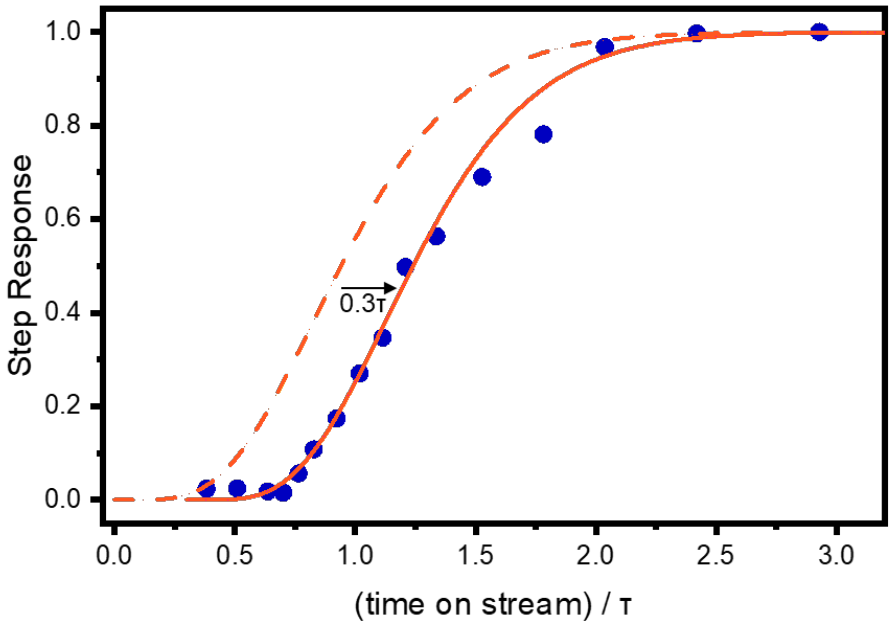

Figure 20. Residence time distribution curve showing response associated with the step change from a DCM solution to a 0.25 M diazo solution at time t = 0 through the packed bed at L = 0.1 mL/min and G = 7 mL/min. The reactor effluent was collected in timepoints and the concentration of diazo in the effluent was monitored via *ex situ* UV vis spectroscopy. The absorbance peak was normalized to the maximum diazo concentration of the step response (0.25 M). Fitting to an nCSTR model gives n = 6. Shifting the fit curve to the right by 0.3 residence times captures the phenomenon of adsorption of diazo to the silica in the packed bed.

With the optimized conditions in hand, we next explored the performance of the process during a continuous flow procedure over a longer time scale. **Figure 21A** shows the conversion of hydrazone starting material and selectivity for diazo product over 10.8 residence times using the following conditions: G = 7 mL/min, L = 0.1 mL/min, and C = 0.25 M. These results show that the complete conversion of hydrazone was maintained over the entire time on stream. However, as the time on stream progressed, the selectivity for diazo product decreased gradually from 100% to a steady state selectivity of 90% after 4.5 residence times. NMR analysis showed that some byproduct formation was due to an O–H insertion reaction between water and the diazo product (likely due to the build-up of

water as an oxidation byproduct as the reaction progressed), as well as some dimerization of the diazo. The turnover number (TON) of the copper catalyst was calculated as:

$$TON = \frac{mmol\ diazo\ produced}{(mmol\ Cu(OAc)_2 \cdot H_2O)\ /\ 2} \quad (6)$$

The TON was determined to be 74. **Figure 21B** shows the elution of each compound from the reactor over time. Diazo concentration reaches its steady state value of 0.23 M at 3.2 residence times. DMAP begins to elute from the column after 8.3 residence times with a final concentration of 0.29 M at 10.8 residence times. This concentration is higher than that of the DMAP in the reaction solution (0.075 M). Therefore, the delayed elution is likely due to polar interactions between DMAP and the silica surface, which slow the travel of DMAP through the packed bed in an effect similar to column chromatography. The retention of DMAP within the silica bed supports the validity of employing the freshly synthesized diazo compound in a downstream dirhodium-carbene reaction without poisoning the Rh_2L_4 catalyst for a time on stream of less than 8.3 residence times. Some Cu leaching (about 5 ppm) was observed throughout most of the reaction progress; however, the Cu largely does not elute from the column until longer time scales, with the timepoints at 9.5 residence times containing 25 ppm of copper and 10.8 residence times containing 82 ppm of copper. Again, this delayed elution is likely due to the interaction of the Cu catalyst with the polar silica surface. The strong interaction between the Cu and silica for extended times also corroborates our earlier observations seen during the split test shown in **Figure 17** and lends further evidence to the possibility of a silica-sorbed Cu precatalyst.

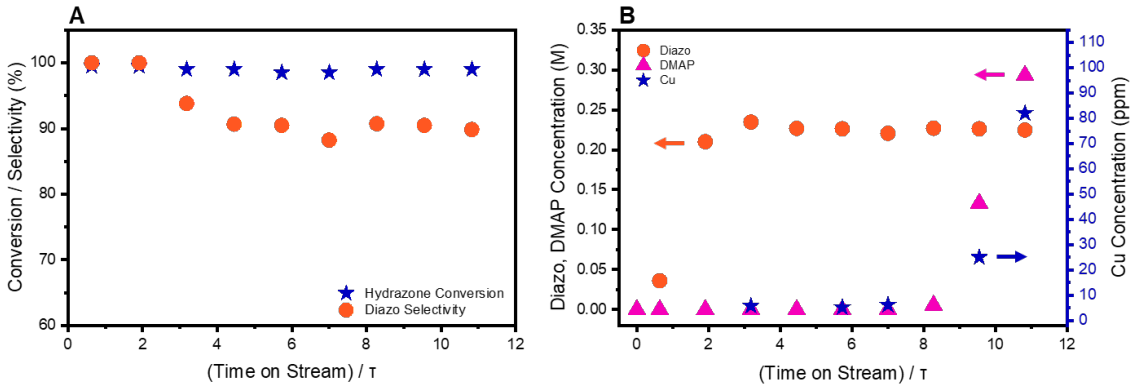

Figure 21. Performance of hydrazone oxidation process over 10.8 residence times. (A) Complete hydrazone conversion is maintained throughout time on stream and steady state diazo selectivity reaches 90% at 4.5 residence times. Hydrazone conversion and diazo selectivity were calculated via quantitative NMR using dodecane as an internal standard. (B) Elution of reaction components from the reactor. Diazo concentration in the effluent was calculated via quantitative NMR using dodecane as an internal standard and was confirmed by integrating the RTD shown in Figure 5; DMAP concentration was calculated via quantitative NMR using dodecane as an internal standard; Cu concentration was quantified using ICP-OES elemental analysis.

3.3.4 Semi-batch dirhodium(II) carbene reactions for immediate consumption of diazo intermediate

Building upon our continuous process, we included a semi-batch, dirhodium-carbene reaction for immediate consumption of the diazo compound downstream of the flow reaction. The semi-batch setup and Rh_2L_4 catalyst structures we employed are shown in **Figure 22A**. To conduct the semi-batch reactions, a round bottom flask was equipped with the appropriate substrate and 1 mol% of the Rh_2L_4 catalyst, along with activated 4Å molecular sieves to capture water that may interfere with the carbene reaction, and connected to the flow reactor effluent.

We performed several different dirhodium-carbene reactions to probe the robustness of this continuous process, as shown in **Figure 22B**. An asymmetric

cyclopropanation reaction with styrene gave a very high yield of 94% and enantioselectivity of 94% ee (**28**). This result is an improvement over the 67% yield observed in the tandem batch reaction employed in the previous Davies, Stahl work,[88] which demonstrates the utility of this continuous process over batch reactions in series. Similarly, a cyclopropenation with ethynylbenzene gave a good yield of 86% and high enantioselectivity of 92% ee (**29**).

Cyclohexa-1,4-diene was used as an activated substrate for secondary C–H insertion (**30**). Moderate yield (64%) and enantioselectivity (71% ee) were observed. Previous studies have shown that addition of 1,1,1,3,3,3-hexafluoro-2-propanol (HFIP) improved reaction performance in dirhodium carbene-catalyzed reactions.[118, 119] The addition of 20 equivalents of HFIP to the semi-batch reaction mixture resulted in an increased C–H insertion yield of 81% and higher selectivity of 83% ee. Finally, we explored the performance of secondary C–H insertion using an unactivated substrate, in this case cyclohexane (**31**). At room temperature, the reaction had excellent enantioselectivity of 99% ee, albeit with a low yield of 32% due to carbene dimer formation as a significant byproduct. Increasing the temperature of the reaction to 50 °C increased the yield slightly to 51%; however, the higher temperature was detrimental to the enantioselectivity, which decreased dramatically to 52% ee. The dirhodium-catalyzed C–H insertion of unactivated substrates is highly sensitive to the reaction condition. For this system, the presence of water and trace DMAP in the solution necessitates further optimization to promote the C–H insertion, and further substrates were not employed in this initial work.

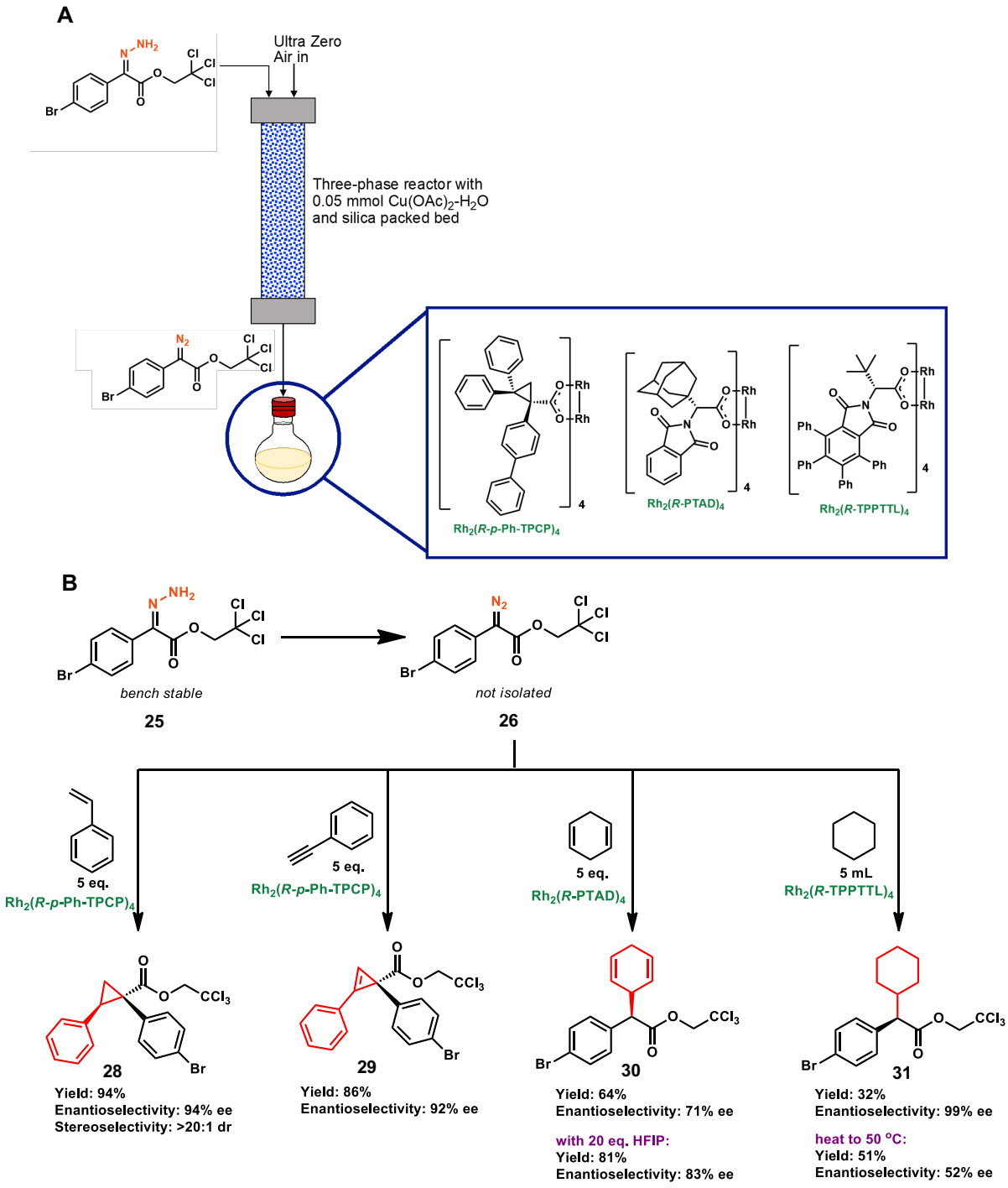

Figure 22. (A) Semi-batch set-up showing the connection of the flow reactor effluent to a round bottom flask containing the appropriate substrate, Rh_2L_4 catalyst, and activated 4 Å molecular sieves. The Rh_2L_4 catalyst structures employed in the C–H insertion reactions are shown. (B) Results of the semi-batch reaction scope. Each reaction was performed at room temperature using 1 mol% of Rh_2L_4 catalyst and 5 equivalents of substrate, unless

otherwise noted. The isolated yield is calculated relative to the 0.25 mmol of hydrazone fed into the flow reactor.

3.4 Conclusion

In this study, we developed a catalytic flow process for the aerobic oxidation of hydrazone to diazo compounds. Our three-phase reactor utilizes co-current downflow of air and liquid streams through a packed bed of silica and $Cu(OAc)_2$-H_2O precatalyst. The performance of the flow system was strongly dependent on air and liquid flow rates, which influenced the hydrodynamics within the packed bed, with a high ratio of air to liquid flow rate important for maximizing diazo yield. A time on stream experiment showed that DMAP and Cu did not begin to elute from the column until 9 residence times. Successful process performance was maintained over 10.8 residence times, with complete hydrazone conversion for the entire time on stream and a steady-state diazo selectivity of 90%. Finally, we employed our flow process upstream of several semi-batch, dirhodium-catalyzed reactions for immediate consumption of the freshly synthesized diazo. This continuous process showed high yield and enantioselectivity for cyclopropanation, cyclopropenation, and activated secondary C–H insertion reactions.

CHAPTER 4. CONCLUSIONS AND RECOMMENDATIONS

4.1 Conclusions and broader impact

In the past two decades, C–H functionalization has created a paradigm shift for organic synthesis by affording new methods to synthesize complex natural products and pharmaceutical molecules.[1, 3, 9-12, 120, 121] In particular, dirhodium carbenes derived from donor/acceptor diazo compounds are synthetically useful, as the thermodynamically favorable evolution of nitrogen gas enables the ready formation of these highly reactive and selective reagents while forming an environmentally benign byproduct. While dirhodium carbenes may offer enhanced process efficiency, their implementation in industrial pharmaceutical processing has been limited due to the high cost of the homogeneous dirhodium catalysts[23] and safety concerns with handling large amounts of highly energetic diazo compounds.[31-33] The work described in this thesis aims to remediate some of these challenges through strategic implementation of packed bed reactors and continuous processing.

Chapter 2 details the heterogenization of the Rh_2(*S*-2-Cl-5-CF_3TPCP)$_4$ catalyst. Based on previous findings from my collaborators,[35] this catalyst was successfully immobilized via an inert tether covalently bonded via [3+2]alkyne-azide cycloaddition to the catalyst's equatorial ligand, preserving accessibility to both catalyst active sites. A quasi-2-dimensional, mesoporous platelet SBA-15 was employed as a support material for the catalyst, as the short pore length limited mass transfer limitations to and from the catalyst immobilized within the pores.

The immobilized Rh_2(*S*-2-Cl-5-CF_3TPCP)$_4$ catalyst was implemented in a packed bed, using HMDS-capped silica as an inert diluent to mitigate pressure drop caused by the small particle size of the platelet SBA-15. The performance of the immobilized catalyst employed in the packed bed was similar to that of the homogeneous catalyst employed in a batch configuration. The process achieved unactivated secondary C–H insertion reactions with high yield and regio-, stereo-, and enantiomeric selectivity. Additionally, process performance was maintained over 10 recycles, although a slight decrease in yield and regioselectivity indicated slow catalyst deactivation over time. The immobilization of the Rh_2(TPCP)$_4$ catalysts resulted in a lower TON due to the introduction of mass transfer limitations, which lowered the overall reaction rate, and catalyst deactivation, which limited recyclability. These features may limit the industrial application of this immobilization technique, and future work investigating heterogenization of Rh_2L_4 catalysts may benefit from studying the catalyst stability and deactivation pathway, as discussed in **Section 4.2.1**.

Chapter 3 details the implementation of a catalytic, aerobic oxidation reaction for the synthesis of diazo compounds in a three-phase packed bed reactor. The system performance was strongly dependent on air and liquid flow rates, which influenced the hydrodynamics within the packed bed. Operating at a high ratio of air to liquid flow rates was important to achieve a high diazo yield. At these conditions, the hydrodynamics within the packed bed correspond to a gas-continuous flow regime with a thin liquid film over the catalyst particles, which is analogous to trickle flow in a macroscale reactor. These insights were used to optimize flow conditions to achieve complete conversion of hydrazone and maximize diazo yield.

A residence time distribution (RTD) at these conditions was then generated and fit to an nCSTR model. The model showed a deviation from ideal plug-flow behavior, likely due to channeling of air and liquid streams causing axial dispersion within the packed bed. Process performance was evaluated over 11 residence times, and complete hydrazone conversion was maintained over the entire process with a steady state diazo selectivity of 90%. Quantitative ^{1}H-NMR spectroscopy and ICP-OES elemental analysis showed that DMAP and Cu, respectively, do not elute from the packed bed until after 9 residence times. Finally, the effluent of the packed bed was connected in series to a semi-batch dirhodium-carbene reaction to achieve immediate consumption of the diazo compound in a downstream reaction. A small reaction scope showed that the process offers high yield for cyclopropanation, cyclopropenation, and secondary C–H insertion with an activated substrate. However, secondary C–H insertion with an unactivated substrate, which is highly sensitive to the reaction condition, was not successful, likely due to the presence of water and trace amounts of DMAP.

To the best of our knowledge, the process described in **Chapter 3** is the first example of a catalytic, aerobic oxidation of hydrazone compounds to achieve diazo synthesis in flow. The successful implementation of this system absolves some shortcomings of other previously published methods to synthesize diazo compounds in flow, which typically generate stoichiometric byproducts, or require strong bases or stoichiometric quantities of metal oxides. In contrast, our system utilizes oxygen (from air) as a sustainable oxidant and generates water as a green byproduct. Additionally, the use of catalytic amounts of copper and high selectivity for diazo product makes this an atom-efficient process that generates low amounts of waste. This, as well as the demonstrated utility of this process to

synthesize diazo compounds as precursors for C–H functionalization reactions, may help alleviate some of the concerns that have prevented industrial adoption of C–H functionalization as a synthetic method due in part to safety concerns associated with handling energetic diazo compounds.

The flow to semi-batch cascade process configuration for dirhodium-carbene reactions may also have promise for industrial processing. The Davies group has demonstrated that homogeneous Rh_2L_4 catalysts may be employed with loadings as low as 0.001 mol% to achieve incredibly high TONs for cyclopropanation reactions.[36] Employing low Rh_2L_4 loadings may represent a more effective strategy than catalyst immobilization to mitigate the Rh cost, as tethering the Rh_2L_4 catalysts to a support results in a lower TON than that of the homogeneous catalyst due to the introduction of mass transfer limitations and catalyst deactivation, which hinders recyclability. However, further optimization of the semi-batch reaction conditions may be required to accommodate lower loadings of the Rh_2L_4 catalyst.

4.2 Recommendations for future work

4.2.1 Further investigation into the deactivation of the immobilized dirhodium(II) catalyst

Although the efforts reported herein have demonstrated the successful heterogenization of Rh_2L_4 catalysts, the immobilization of Rh_2L_4 catalysts and their implementation in continuous processes has not led to an increase in TON, as catalyst deactivation over time limits their recyclability. The limitation of these and other prior research efforts is the exhibitionist strategy that aims primarily to demonstrate the

possibility of catalyst heterogenization, rather than to conduct detailed studies of catalyst stability and deactivation.[24, 25, 122] The circumstances that lead to catalyst deactivation represent a fundamental gap in our understanding of molecular catalysis that must be bridged in order to develop more effective catalyst immobilization techniques.

Some seminal studies have shown that many different factors can influence the deactivation of molecular transition metal catalysts. For example, some metal centers may undergo a reduction in oxidation state[123] or they may aggregate to form an inactive dimerized catalyst complex.[124, 125] However, due to the presence of immobilized ligands or coordinated counter ions, the deactivation pathway for molecular catalysts may be more complex. Mack *et al.* recently published a study on the deactivation pathway of a ruthenium catalyst with 4,4′-di-*tert*-butyl-2,2′-bipyridine (dtbpy) ligands that catalyzes the oxidation of C(sp^3)–H bonds. Surprisingly, they found that the dtbpy ligands dissociate from the catalyst complex, undergo oxidation (likely mediated by the ruthenium catalyst), and subsequently poison the catalyst active site.[125] Similar studies have shown that the loss or modification of a ligand or counter ion resulted in catalyst deactivation.[126-128]

Research on catalyst stability has also been used as a method to inform more effective catalyst immobilization and recycle techniques.[24, 25] For example, previous studies from the Jones group showed that catalyst recovery and regeneration procedures contributed to deactivation; these were adjusted to successfully increase catalyst lifetime and recyclability.[126, 127] Other techniques that may be employed to mitigate catalyst deactivation include: implementation of a "scavenger" to selectively remove catalyst poisons, the capture and recycle of leached catalyst ligands, design of more robust materials

for immobilization, and temperature ramp to maintain catalyst activity in the face of irreversible deactivation.[24]

A recent study conducted by the Davies group employed insightful kinetic studies to determine the effect of ligand identity on homogeneous Rh_2L_4 catalyst performance and maximize the TON (100,000) by employing extremely small catalyst loadings (0.001 mol%). Although these catalysts were subjected to very high TON, they did not show signs of deactivation or product inhibition.[36] However, these catalysts were not recycled; thus, deactivation may occur at longer time scales, during the recovery process, or upon reuse. Additionally, the catalyst was employed in batch, so a possibly dissociated ligand will remain in solution and may continue to coordinate with the active catalyst. In contrast, the previously discussed results (**Chapter 2**) showed that the immobilized catalyst experienced a loss in catalytic activity over multiple recycles, although the catalyst was not found to leach from the support. The employment of more rigorous kinetic studies to monitor changes in kinetic performance of homogeneous vs immobilized Rh_2L_4 catalysts over multiple recycles would be invaluable in demonstrating change in catalyst TOF and performance over time. Additionally, employing extensive catalyst characterization before reaction and after several recycles may elucidate changes in catalyst structure or rhodium oxidation state. More specific knowledge about the deactivation pathway of the Rh_2L_4 catalysts would be instrumental in identifying specific creative solutions to maximize the immobilized catalysts' lifetime.

4.2.2 Further improvements to the hydrazone oxidation process

As discussed in **Chapter 3**, while the three-phase packed bed did achieve complete conversion of hydrazone and high yield of diazo product, this initial study could be improved upon with further optimization. Firstly, the reactor employed in this study was shown to exhibit deviation from ideal plug flow behavior, likely due to channeling and axial dispersion in the packed bed.[99] This nonideal behavior may be mitigated by more explicitly modelling the dispersion behavior and revising the design of the column employed in this study. For example, a reactor with a smaller internal diameter (or smaller diameter to length ratio) may exhibit more ideal flow patterns.

While the $Cu(OAc)_2$-H_2O was successfully employed with low leaching in our lab-scale study, this system may not be ideal for industrial-scale continuous processing of pharmaceuticals, as Cu leaching may lower process performance over time and require periodic shutdowns to reload the $Cu(OAc)_2$-H_2O in the column. To this end, identifying a truly heterogeneous catalyst capable of conducting aerobic hydrazone oxidation would greatly improve the practicality of this process for diazo synthesis. Efforts to achieve this goal are currently underway.

Finally, a more expansive semi-batch reaction scope may provide additional insight into the specific limitations of employing this method for diazo synthesis upstream of Rh_2L_4-catalyzed reactions. With this knowledge in hand, certain modifications to the hydrazone oxidation process may expand its utility in downstream dirhodium-carbene reactions. For example, the addition of a purification column upstream of the semi-batch

reaction may be employed to dry and selectively remove pyridyl bases from the reaction stream.

4.2.3 Demonstrate scalability of C–H functionalization process

Further improvements to the hydrazone oxidation process and implementation of immobilized Rh_2L_4 catalysts with higher TON could temper the barriers preventing industrial implementation of C–H functionalization in pharmaceutical synthesis. Future work focusing on the applicability of this chemistry to industrial processing may include more studies surrounding potential scale-up of the hydrazone oxidation and C–H functionalization packed beds, for example by examining process performance in large-scale syntheses or investigating how reactor dimensions influence reaction performance.

Additionally, other methods to employ C–H functionalization in continuous processing may be employed. For example, rather than a semi-batch reaction setup, the homogeneous Rh_2L_4-catalyzed reaction may be employed in flow using a simple plug flow reactor, with injection of the Rh_2L_4 catalyst downstream of the diazo synthesis. Minimizing the Rh loading in this process configuration may be an interesting study for future work to demonstrate the performance of an industrially-feasible continuous process for C–H functionalization. The practicality of such a system could be demonstrated by performing key synthetic steps for specific drugs that are of interest to the pharmaceutical industry.

REFERENCES

1. Godula, K.; Sames, D., C–H Bond Functionalization in Complex Organic Synthesis. *Science* **2006,** *312* (5770), 67-72.

2. Davies, H. M.; Du Bois, J.; Yu, J. Q., C-H functionalization in organic synthesis. *Chem. Soc. Rev.* **2011,** *40* (4), 1855-1856.

3. Davies, H. M.; Morton, D., Recent Advances in C-H Functionalization. *J. Org. Chem.* **2016,** *81* (2), 343-350.

4. Davies, H. M.; Manning, J. R., Catalytic C-H functionalization by metal carbenoid and nitrenoid insertion. *Nature* **2008,** *451* (7177), 417-24.

5. Jimenez-Gonzalez, C.; Constable, D. J.; Ponder, C. S., Evaluating the "greenness" of chemical processes and products in the pharmaceutical industry--a green metrics primer. *Chem. Soc. Rev.* **2012,** *41* (4), 1485-1498.

6. Sheldon, R. A., The E Factor: fifteen years on. *Green Chem.* **2007,** *9* (12), 1273-1278.

7. Jimenez-Gonzalez, C.; Ponder, C. S.; Broxterman, Q. B.; Manley, J. B., Using the Right Green Yardstick: Why Process Mass Intensity Is Used in the Pharmaceutical Industry To Drive More Sustainable Processes. *Org. Process Res. Dev.* **2011,** *15*, 912-917.

8. Vaccaro, L.; Curini, M.; Ferlin, F.; Lanari, D.; Marrocchi, A.; Piermatti, O.; Trombettoni, V., Definition of green synthetic tools based on safer reaction media, heterogeneous catalysis, and flow technology. *Pure Appl. Chem.* **2018,** *90* (1), 21-33.

9. Yamaguchi, J.; Yamaguchi, A. D.; Itami, K., C-H bond functionalization: emerging synthetic tools for natural products and pharmaceuticals. *Angew. Chem. Int. Ed.* **2012,** *51* (36), 8960-9009.

10. Colby, D. A.; Bergman, R. G.; Ellman, J. A., Rhodium-Catalyzed C-C Bond Formation via Heteroatom-Directed C-H Bond Activation. *Chem. Rev.* **2010,** *110*, 624–655.

11. Gutekunst, W. R.; Baran, P. S., C-H functionalization logic in total synthesis. *Chem. Soc. Rev.* **2011,** *40* (4), 1976-1991.

12. Wencel-Delord, J.; Glorius, F., C-H bond activation enables the rapid construction and late-stage diversification of functional molecules. *Nat. Chem.* **2013,** *5*, 369-75.

13. What is C–H functionalization? https://nsf-cchf.com/aboutCHF.html.

14. Liao, K.; Liu, W.; Niemeyer, Z. L.; Ren, Z.; Bacsa, J.; Musaev, D. G.; Sigman, M. S.; Davies, H. M. L., Site-Selective Carbene-Induced C–H Functionalization Catalyzed by Dirhodium Tetrakis(triarylcyclopropanecarboxylate) Complexes. *ACS Catal.* **2018,** *8*, 678-682.

15. Liao, K.; Negretti, S.; Musaev, D. G.; Bacsa, J.; Davies, H. M., Site-selective and stereoselective functionalization of unactivated C-H bonds. *Nature* **2016,** *533*, 230-234.

16. Liao, K.; Pickel, T. C.; Boyarskikh, V.; Bacsa, J.; Musaev, D. G.; Davies, H. M. L., Site-selective and stereoselective functionalization of non-activated tertiary C-H bonds. *Nature* **2017,** *551* (7682), 609-613.

17. Liao, K.; Yang, Y. F.; Li, Y.; Sanders, J. N.; Houk, K. N.; Musaev, D. G.; Davies, H. M. L., Design of catalysts for site-selective and enantioselective functionalization of non-activated primary C-H bonds. *Nat. Chem.* **2018,** *10*, 1048-1055.

18. Davies, H. M. L., Finding Opportunities from Surprises and Failures. Development of Rhodium-Stabilized Donor/Acceptor Carbenes and Their Application to Catalyst-Controlled C-H Functionalization. *J. Org. Chem.* **2019,** *84*, 12722-12745.

19. Kornecki, K. P.; Briones, J. F.; Boyarskikh, V.; Fullilove, F.; Autschbach, J.; Schrote, K. E.; Lancaster, K. M.; Davies, H. M.; Berry, J. F., Direct spectroscopic characterization of a transitory dirhodium donor-acceptor carbene complex. *Science* **2013,** *342*, 351-354.

20. Wilkerson-Hill, S. M.; Davies, H. M., Rhodium (II) TetraCarboxylate-Catalyzed Enantioselective C-H Functionalization Reactions. In *Rhodium Catalysis in Organic Synthesis*, Tanaka, K., Ed. Wiley-VCH: Weinheim, Germany, 2019; pp 341-372.

21. Davies, H. M.; Morton, D., Guiding principles for site selective and stereoselective intermolecular C-H functionalization by donor/acceptor rhodium carbenes. *Chem. Soc. Rev.* **2011,** *40*, 1857-1869.

22. Xiang, Y.; Wang, C.; Ding, Q.; Peng, Y., Diazo Compounds: Versatile Synthons for the Synthesis of Nitrogen Heterocycles via Transition Metal-Catalyzed Cascade C-H Activation/Carbene Insertion/Annulation Reactions. *Adv. Synth. Catal.* **2019,** *361*, 919-944.

23. Gandeepan, P.; Muller, T.; Zell, D.; Cera, G.; Warratz, S.; Ackermann, L., 3d Transition Metals for C-H Activation. *Chem. Rev.* **2019,** *119*, 2192-2452.

24. Scott, S. L., A Matter of Life(time) and Death. *ACS Catal.* **2018,** *8*, 8597-8599.

25. Jones, C. W., On the Stability and Recyclability of Supported Metal–Ligand Complex Catalysts: Myths, Misconceptions and Critical Research Needs. *Topics in Catalysis* **2010,** *53* (13), 942-952.

26. Vos, D. E. D.; Dams, M.; Sels, B. F.; Jacobs, P. A., Ordered Mesoporous and Microporous Molecular Sieves Functionalized with Transition Metal Complexes as Catalysts for Selective Organic Transformations. *Chem. Rev.* **2002,** *102*, 3615-3640.

27. Zhao, X. S.; Bao, X. Y.; Guo, W.; Lee, F. Y., Immobilizing catalysts on porous materials. *Mater. Today* **2006,** *9* (3), 32-39.

28. Shylesh, S.; Schunemann, V.; Thiel, W. R., Magnetically separable nanocatalysts: bridges between homogeneous and heterogeneous catalysis. *Angew. Chem. Int. Ed.* **2010,** *49*, 3428-3459.

29. Collis, A. E. C.; Horváth, I. T., Heterogenization of homogeneous catalytic systems. *Catal. Sci. Technol.* **2011,** *1*, 912-919.

30. Alonso, A.; Shafir, A.; Macanás, J.; Vallribera, A.; Muñoz, M.; Muraviev, D. N., Recyclable polymer-stabilized nanocatalysts with enhanced accessibility for reactants. *Catal. Today* **2012,** *193* (1), 200-206.

31. Green, S. P.; Wheelhouse, K. M.; Payne, A. D.; Hallett, J. P.; Miller, P. W.; Bull, J. A., Thermal Stability and Explosive Hazard Assessment of Diazo Compounds and Diazo Transfer Reagents. *Org. Process Res. Dev.* **2020,** *24*, 67-84.

32. Deadman, B. J.; Collins, S. G.; Maguire, A. R., Taming hazardous chemistry in flow: the continuous processing of diazo and diazonium compounds. *Chem. Eur. J.* **2015,** *21*, 2298-2308.

33. Muller, S. T.; Wirth, T., Diazo compounds in continuous-flow technology. *ChemSusChem* **2015,** *8* (2), 245-50.

34. Pereira, C. J.; Leib, T. M., Reactors. In *Perry's Chemical Engineers' Handbook*, 8 ed.; Green, D. W., Ed. The McGraw-Hill Companies, Inc.: 2008; pp 14-18.

35. Hatridge, T. A.; Liu, W.; Yoo, C. J.; Davies, H. M. L.; Jones, C. W., Optimized Immobilization Strategy for Dirhodium(II) Carboxylate Catalysts for C-H Functionalization and Their Implementation in a Packed Bed Flow Reactor. *Angew. Chem. Int. Ed.* **2020,** *132*, 19693-12699.

36. Wei, B.; Sharland, J. C.; Lin, P.; Wilkerson-Hill, S. M.; Fullilove, F. A.; McKinnon, S.; Blackmond, D. G.; Davies, H. M. L., In Situ Kinetic Studies of Rh(II)-Catalyzed Asymmetric Cyclopropanation with Low Catalyst Loadings. *ACS Catal.* **2019,** *10*, 1161-1170.

37. Davies, H. M.; Walji, A. M.; Nagashima, T., Simple Strategy for the Immobilization of Dirhodium Tetraprolinate Catalysts Using a Pyridine-Linked Solid Support. *J. Am. Chem. Soc.* **2004,** *126*, 4271-4280.

38. Davies, H. M.; Walji, A. M., Asymmetric Intermolecular C−H Activation, Using Immobilized Dirhodium Tetrakis((S)-N-(dodecylbenzenesulfonyl)- prolinate) as a Recoverable Catalyst. *Org. Lett.* **2003,** *5* (4), 479-482.

39. Davies, H. M.; Walji, A. M., Universal Strategy for the Immobilization of Chiral Dirhodium Catalysts. *Org. Lett.* **2005,** *7* (14), 2941-2944.

40. Takeda, K.; Oohara, T.; Anada, M.; Nambu, H.; Hashimoto, S., A polymer-supported chiral dirhodium(II) complex: highly durable and recyclable catalyst for asymmetric intramolecular C-H insertion reactions. *Angew. Chem.* **2010,** *122*, 7133-7137.

41. Takeda, K.; Oohara, T.; Shimada, N.; Nambu, H.; Hashimoto, S., Continuous flow system with a polymer-supported dirhodium(II) catalyst: application to enantioselective carbonyl ylide cycloaddition reactions. *Chem. Eur. J.* **2011,** *17* (50), 13992-13998.

42. Chepiga, K. M.; Feng, Y.; Brunelli, N. A.; Jones, C. W.; Davies, H. M., Silica-Immobilized Chiral Dirhodium(II) Catalyst for Enantioselective Carbenoid Reactions. *Org. Lett.* **2013,** *15* (24), 6136-6139.

43. Moschetta, E. G.; Negretti, S.; Chepiga, K. M.; Brunelli, N. A.; Labreche, Y.; Feng, Y.; Rezaei, F.; Lively, R. P.; Koros, W. J.; Davies, H. M.; Jones, C. W., Composite polymer/oxide hollow fiber contactors: versatile and scalable flow reactors for heterogeneous catalytic reactions in organic synthesis. *Angew. Chem. Int. Ed.* **2015,** *54*, 6470-6474.

44. Yoo, C. J.; Rackl, D.; Liu, W.; Hoyt, C. B.; Pimentel, B.; Lively, R. P.; Davies, H. M. L.; Jones, C. W., An Immobilized-Dirhodium Hollow-Fiber Flow Reactor for Scalable and Sustainable C-H Functionalization in Continuous Flow. *Angew. Chem. Int. Ed.* **2018,** *57*, 10923-10927.

45. Liu, W.; Ren, Z.; Bosse, A. T.; Liao, K.; Goldstein, E. L.; Bacsa, J.; Musaev, D. G.; Stoltz, B. M.; Davies, H. M. L., Catalyst-Controlled Selective Functionalization of Unactivated C-H Bonds in the Presence of Electronically Activated C-H Bonds. *J. Am. Chem. Soc.* **2018,** *140*, 12247-12255.

46. Liu, W.; Babl, T.; Rother, A.; Reiser, O.; Davies, H. M. L., Functionalization of Piperidine Derivatives for the Site-Selective and Stereoselective Synthesis of Positional Analogues of Methylphenidate. *Chem. Eur. J.* **2020,** *26*, 4236-4241.

47. Guptill, D. M.; Davies, H. M., 2,2,2-Trichloroethyl aryldiazoacetates as robust reagents for the enantioselective C-H functionalization of methyl ethers. *J. Am. Chem. Soc.* **2014,** *136*, 17718-17721.

48. Zhang, H.; Sun, J.; Ma, D.; Weinberg, G.; Su, D. S.; Bao, X., Engineered Complex Emulsion System: Toward Modulating the Pore Length and Morphological Architecture of Mesoporous Silicas. *J. Phys. Chem. B* **2006,** *110* (51), 25908-25915.

49. Godula, K.; Rabuka, D.; Nam, K. T.; Bertozzi, C. R., Synthesis and microcontact printing of dual end-functionalized mucin-like glycopolymers for microarray applications. *Angew. Chem.* **2009,** *48* (27), 4973-6.

50. Chandra, P.; Jonas, A. M.; Fernandes, A. E., Sequence and Surface Confinement Direct Cooperativity in Catalytic Precision Oligomers. *J. Am. Chem. Soc.* **2018,** *140*, 5179-5184.

51. Qin, C.; Boyarskikh, V.; Hansen, J. H.; Hardcastle, K. I.; Musaev, D. G.; Davies, H. M., D2-symmetric dirhodium catalyst derived from a 1,2,2-triarylcyclopropanecarboxylate ligand: design, synthesis and application. *J. Am. Chem. Soc.* **2011,** *133*, 19198-19204.

52. Qin, C.; Davies, H. M., Role of sterically demanding chiral dirhodium catalysts in site-selective C-H functionalization of activated primary C-H bonds. *J. Am. Chem. Soc.* **2014,** *136*, 9792-9796.

53. McCabe, W. L.; Smith, J. S.; P., H., Chapter 7: Flow Past Immersed Objects. In *Unit Operations of Chemical Engineering, 7th edition*, McGraw Hill: 2005; p 166.

54. Badger, G. M.; Sasse, W. H. F., The Action of Metal Catalysts on Pyridines. In *Advances in Heterocyclic Chemistry Volume 2*, 1963; pp 179-202.

55. Tanabe, K.; Hölderich, W. F., Industrial application of solid acid—base catalysts. *Appl. Catal. A-Gen.* **1999,** *181*, 399-434.

56. Lin, T. B.; Chung, D. L.; Chang, J. R., Ethyl Acetate Production from Water-Containing Ethanol Catalyzed by Supported Pd Catalysts: Advantages and Disadvantages of Hydrophobic Supports. *Ind. Eng. Chem. Res.* **1999,** *38*, 1271-1276.

57. Sakthivel, A.; Badamali, S. K.; Selvam, P., para-Selective t-butylation of phenol over mesoporous H-AlMCM-41. *Micropor. Mesopor. Mat.* **2000,** *39*, 457-463.

58. Li, B.; Yan, R.; Wang, L.; Diao, Y.; Li, Z.; Zhang, S., SBA-15 Supported Cesium Catalyst for Methyl Methacrylate Synthesis via Condensation of Methyl Propionate with Formaldehyde. *Ind. Eng. Chem. Res.* **2014,** *53*, 1386-1394.

59. Wang, Q.-N.; Shi, L.; Lu, A.-H., Highly Selective Copper Catalyst Supported on Mesoporous Carbon for the Dehydrogenation of Ethanol to Acetaldehyde. *ChemCatChem* **2015,** *7* (18), 2846-2852.

60. Li, Z.; Peters, A. W.; Bernales, V.; Ortuno, M. A.; Schweitzer, N. M.; DeStefano, M. R.; Gallington, L. C.; Platero-Prats, A. E.; Chapman, K. W.; Cramer, C. J.; Gagliardi, L.; Hupp, J. T.; Farha, O. K., Metal-Organic Framework Supported Cobalt Catalysts for the Oxidative Dehydrogenation of Propane at Low Temperature. *ACS Cent. Sci.* **2017,** *3*, 31-38.

61. Carceller, J. M.; Mifsud, M.; Climent, M. J.; Iborra, S.; Corma, A., Production of chiral alcohols from racemic mixtures by integrated heterogeneous chemoenzymatic catalysis in fixed bed continuous operation. *Green Chem.* **2020,** *22*, 2767-2777.

62. Wang, D.; Szabo, K. J., Copper-Catalyzed, Stereoselective Cross-Coupling of Cyclic Allyl Boronic Acids with alpha-Diazoketones. *Org. Lett.* **2017,** *19* (7), 1622-1625.

63. Xia, Y.; Qiu, D.; Wang, J., Transition-Metal-Catalyzed Cross-Couplings through Carbene Migratory Insertion. *Chem. Rev.* **2017,** *117* (23), 13810-13889.

64. Zhang, B.; Davies, H. M. L., Rhodium-Catalyzed Enantioselective [4+2] Cycloadditions of Vinylcarbenes with Dienes. *Angew. Chem.* **2020,** *132*, 4967-4971.

65. Negretti, S.; Cohen, C. M.; Chang, J. J.; Guptill, D. M.; Davies, H. M. L., Enantioselective Dirhodium(II)-Catalyzed Cyclopropanations with Trimethylsilylethyl and Trichloroethyl Aryldiazoacetates. *Tetrahedron* **2015,** *71*, 7415-7420.

66. Gillingham, D.; Fei, N., Catalytic X-H insertion reactions based on carbenoids. *Chem. Soc. Rev.* **2013,** *42* (12), 4918-4931.

67. Harada, S.; Tanikawa, K.; Homma, H.; Sakai, C.; Ito, T.; Nemoto, T., Silver-Catalyzed Asymmetric Insertion into Phenolic O-H Bonds using Aryl Diazoacetates and Theoretical Mechanistic Studies. *Chem. Eur. J.* **2019,** *25*, 12058-12062.

68. Tanbouza, N.; Keipour, H.; Ollevier, T., FeII-catalysed insertion reaction of α-diazocarbonyls into X–H bonds (X = Si, S, N, and O) in dimethyl carbonate as a suitable solvent alternative. *RSC Adv.* **2019,** *9*, 31241-31246.

69. Davies, H. M.; Liao, K., Dirhodium tetracarboxylates as catalysts for selective intermolecular C–H functionalization. *Nat. Rev. Chem.* **2019,** *3*, 347−360.

70. Sullivan, R. J.; Freure, G. P. R.; Newman, S. G., Overcoming Scope Limitations in Cross-Coupling of Diazo Nucleophiles by Manipulating Catalyst Speciation and Using Flow Diazo Generation. *ACS Catal.* **2019,** *9* (6), 5623-5630.

71. Muller, S. T.; Murat, A.; Maillos, D.; Lesimple, P.; Hellier, P.; Wirth, T., Rapid Generation and Safe Use of Carbenes Enabled by a Novel Flow Protocol with In-line IR spectroscopy. *Chem. Eur. J.* **2015,** *21* (19), 7016-7020.

72. Deadman, B. J.; O'Mahony, R. M.; Lynch, D.; Crowley, D. C.; Collins, S. G.; Maguire, A. R., Taming tosyl azide: the development of a scalable continuous diazo transfer process. *Org. Biomol. Chem.* **2016,** *14* (13), 3423-3431.

73. Yu, Z.; Dong, H.; Xie, X.; Liu, J.; Su, W., Continuous-Flow Diazotization for Efficient Synthesis of Methyl 2-(Chlorosulfonyl)benzoate: An Example of Inhibiting Parallel Side Reactions. *Org. Process Res. Dev.* **2016,** *20*, 2116-2123.

74. Audubert, C.; Gamboa Marin, O. J.; Lebel, H., Batch and Continuous-Flow One-Pot Processes using Amine Diazotization to Produce Silylated Diazo Reagents. *Angew. Chem. Int. Ed.* **2017,** *56* (22), 6294-6297.

75. Pieber, B.; Kappe, C. O., Generation and Synthetic Application of Trifluoromethyl Diazomethane Utilizing Continuous Flow Technologies. *Org. Lett.* **2016,** *18* (5), 1076-1079.

76. Lehmann, H., A scalable and safe continuous flow procedure for in-line generation of diazomethane and its precursor MNU. *Green Chem.* **2017,** *19* (6), 1449-1453.

77. Levesque, E.; Laporte, S. T.; Charette, A. B., Continuous Flow Synthesis and Purification of Aryldiazomethanes through Hydrazone Fragmentation. *Angew. Chem.* **2017,** *129*, 855-859.

78. Maurya, R. A.; Park, C. P.; Lee, J. H.; Kim, D. P., Continuous in situ generation, separation, and reaction of diazomethane in a dual-channel microreactor. *Angew. Chem. Int. Ed.* **2011,** *50*, 5952-5955.

79. Mastronardi, F.; Gutmann, B.; Kappe, C. O., Continuous Flow Generation and Reactions of Anhydrous Diazomethane Using a Teflon AF-2400 Tube-in-Tube Reactor. *Org. Lett.* **2013,** *15* (21), 5590–5593.

80. Wernik, M.; Poechlauer, P.; Schmoelzer, C.; Dallinger, D.; Kappe, C. O., Design and Optimization of a Continuous Stirred Tank Reactor Cascade for Membrane-Based Diazomethane Production: Synthesis of α-Chloroketones. *Org. Proc. Res. & Dev.* **2019,** *23*, 1359-1368.

81. Sheeran, J. W.; Campbell, K.; Breen, C. P.; Hummel, G.; Huang, C.; Datta, A.; Boyer, S. H.; Hecker, S. J.; Bio, M. M.; Fang, Y.-Q.; Ford, D. D.; Russell, M. G., Scalable On-Demand Production of Purified Diazomethane Suitable for Sensitive Catalytic Reactions. *Org. Process Res. Dev.* **2021,** *25* (3), 522-528.

82. Poh, J. S.; Tran, D. N.; Battilocchio, C.; Hawkins, J. M.; Ley, S. V., A Versatile Room-Temperature Route to Di- and Trisubstituted Allenes Using Flow-Generated Diazo Compounds. *Angew. Chem. Int. Ed.* **2015,** *54* (27), 7920-7923.

83. Roda, N. M.; Tran, D. N.; Battilocchio, C.; Labes, R.; Ingham, R. J.; Hawkins, J. M.; Ley, S. V., Cyclopropanation using flow-generated diazo compounds. *Org. Biomol. Chem.* **2015,** *13* (9), 2550-2554.

84. Tran, D. N.; Battilocchio, C.; Lou, S. B.; Hawkins, J. M.; Ley, S. V., Flow chemistry as a discovery tool to access sp(2)-sp(3) cross-coupling reactions via diazo compounds. *Chem. Sci.* **2015,** *6* (2), 1120-1125.

85. Poh, J. S.; Makai, S.; von Keutz, T.; Tran, D. N.; Battilocchio, C.; Pasau, P.; Ley, S. V., Rapid Asymmetric Synthesis of Disubstituted Allenes by Coupling of Flow-

Generated Diazo Compounds and Propargylated Amines. *Angew. Chem. Int. Ed.* **2017,** *56* (7), 1864-1868.

86. Rackl, D.; Yoo, C. J.; Jones, C. W.; Davies, H. M. L., Synthesis of Donor/Acceptor-Substituted Diazo Compounds in Flow and Their Application in Enantioselective Dirhodium-Catalyzed Cyclopropanation and C-H Functionalization. *Org. Lett.* **2017,** *19* (12), 3055-3058.

87. Nicolle, S. M.; Hayes, C. J.; Moody, C. J., Alkyl halide-free heteroatom alkylation and epoxidation facilitated by a recyclable polymer-supported oxidant for the in-flow preparation of diazo compounds. *Chem. Eur. J.* **2015,** *21* (12), 4576-4579.

88. Liu, W.; Twilton, J.; Wei, B.; Lee, M.; Hopkins, M. N.; Bacsa, J.; Stahl, S. S.; Davies, H. M. L., Copper-Catalyzed Oxidation of Hydrazones to Diazo Compounds Using Oxygen as the Terminal Oxidant. *ACS Catal.* **2021,** *11* (5), 2676-2683.

89. Davies, H. M.; Hansen, T.; Churchill, M. R., Catalytic Asymmetric C-H Activation of Alkanes and Tetrahydrofuran. *J. Am. Chem. Soc.* **2000,** *122*, 3063-3070.

90. Zhao, X.; Zhang, Y.; Wang, J., Recent developments in copper-catalyzed reactions of diazo compounds. *Chem. Commun.* **2012,** *48* (82), 10162-10173.

91. Gavriilidis, A.; Constantinou, A.; Hellgardt, K.; Hii, K. K.; Hutchings, G. J.; Brett, G. L.; Kuhn, S.; Marsden, S. P., Aerobic oxidations in flow: opportunities for the fine chemicals and pharmaceuticals industries. *React. Chem. Eng.* **2016,** *1* (6), 595-612.

92. Greene, J. F.; Hoover, J. M.; Mannel, D. S.; Root, T. W.; Stahl, S. S., Continuous-Flow Aerobic Oxidation of Primary Alcohols with a Copper(I)/TEMPO Catalyst. *Org. Process Res. Dev.* **2013,** *17* (10), 1247-1251.

93. Vanoye, L.; Aloui, A.; Pablos, M.; Philippe, R.; Percheron, A.; Favre-Reguillon, A.; Bellefon, C. d., A Safe and Efficient Flow Oxidation of Aldehydes with O2. *Org. Lett.* **2013,** *15* (23), 5978-5981.

94. He, Z.; Jamison, T. F., Continuous-flow synthesis of functionalized phenols by aerobic oxidation of Grignard reagents. *Angew. Chem. Int. Ed.* **2014,** *53* (13), 3353-3357.

95. Greene, J. F.; Preger, Y.; Stahl, S. S.; Root, T. W., PTFE-Membrane Flow Reactor for Aerobic Oxidation Reactions and Its Application to Alcohol Oxidation. *Org. Process Res. Dev.* **2015,** *19* (7), 858-864.

96. Al-Rifai, N.; Galvanin, F.; Morad, M.; Cao, E.; Cattaneo, S.; Sankar, M.; Dua, V.; Hutchings, G.; Gavriilidis, A., Hydrodynamic effects on three phase micro-packed bed reactor performance – Gold–palladium catalysed benzyl alcohol oxidation. *Chem. Eng. Sci.* **2016,** *149*, 129-142.

97. Pintar, A.; Bercic, G.; Levec, J., Catalytic liquid-phase oxidation of aqueous phenol solutions in a trickle-bed reactor. *Chem. Eng. Sci.* **1997,** *52*, 4143-4153.

98. Mata, A. R.; Smith, J. M., Oxidation of Sulfur Dioxide in a Trickle-bed Reactor. *Chem. Eng. J.* **1981,** *22*, 229-235.

99. Ranade, V. V.; Chaudhari, R. V.; Gunjal, P. R., Hydrodynamics and Flow Regimes. In *Trickle Bed Reactors*, Elsevier: 2011; pp 25-75.

100. Losey, M. W.; Schmidt, M. A.; Jensen, K. F., Microfabricated Multiphase Packed-Bed Reactors: Characterization of Mass Transfer and Reactions. *Ind. Eng. Chem. Res.* **2001,** *40* (12), 2555-2562.

101. Yue, J.; Chen, G.; Yuan, Q.; Luo, L.; Gonthier, Y., Hydrodynamics and mass transfer characteristics in gas–liquid flow through a rectangular microchannel. *Chem. Eng. Sci.* **2007,** *62* (7), 2096-2108.

102. Alsolami, B. H.; Berger, R. J.; Makkee, M.; Moulijn, J. A., Catalyst Performance Testing in Multiphase Systems: Implications of Using Small Catalyst Particles in Hydrodesulfurization. *Ind. Eng. Chem. Res.* **2013,** *52* (26), 9069-9085.

103. Qin, C.; Davies, H. M., Rh2(R-TPCP)4-catalyzed enantioselective [3+2]-cycloaddition between nitrones and vinyldiazoacetates. *J. Am. Chem. Soc.* **2013,** *135* (39), 14516-14519.

104. Reddy, R. P.; Lee, G. H.; Davies, H. M. L., Dirhodium Tetracarboxylate Derived from Adamantylglycine as a Chiral Catalyst for Carbenoid Reactions. *Org. Lett.* **2006,** *8* (16), 3437-3440.

105. Fu, J.; Ren, Z.; Bacsa, J.; Musaev, D. G.; Davies, H. M. L., Desymmetrization of cyclohexanes by site- and stereoselective C-H functionalization. *Nature* **2018,** *564* (7736), 395-399.

106. Genelot, M.; Dufaud, V.; Djakovitch, L., Carbonylative Sonogashira Coupling in the Synthesis of Ynones: A Study of "Boomerang" Phenomena. *Adv. Synth. Catal.* **2013,** *355* (13), 2604-2616.

107. Al-Dahhan, M. H.; Wu, Y.; Dudukovic, M. P., Reproducible Technique for Packing Laboratory-Scale Trickle-Bed Reactors with a Mixture of Catalyst and Fines. *Ind. Eng. Chem. Res.* **1995,** *34*, 741-747.

108. Likhar, P. R.; Roy, S.; Roy, M.; Kantam, M. L.; De, R. L., Silica immobilized copper complexes: Efficient and reusable catalysts for N-arylation of N(H)-heterocycles and benzyl amines with aryl halides and arylboronic acids. *J. Mol. Catal. A: Chem.* **2007,** *271*, 57-62.

109. Donia, A. M.; Atia, A. A.; El-Boraey, H.; Mabrouk, D. H., Uptake studies of copper(II) on glycidyl methacrylate chelating resin containing Fe2O3 particles. *Sep. Purif. Technol.* **2006,** *49*, 64-70.

110. Wu, X.; Gorden, A. E. V., 2-Quinoxalinol salen ligands incorporated into functionalized resins for selective solid-phase extraction of copper(II). *Tetrahedron Lett.* **2008,** *49* (35), 5200-5203.

111. Musaev, D. G.; Liebeskind, L. S., On the Mechanism of Pd(0)-Catalyzed, Cu(I) Carboxylate-Mediated Thioorganic-Boronic Acid Desulfitative Coupling. A Non-innocent Role for Carboxylate Ligand. *Organometallics* **2009,** *28*, 4639-4642.

112. Gruttadauria, M.; Giacalone, F.; Noto, R., "Release and catch" catalytic systems. *Green Chem.* **2013,** *15*, 2608-2618.

113. Weissman, S. A.; Anderson, N. G., Design of Experiments (DoE) and Process Optimization. A Review of Recent Publications. *Org. Process Res. Dev.* **2014,** *19* (11), 1605-1633.

114. Long, B.; Ryan, K. M.; Padrela, L., Investigating Process Variables and Additive Selection To Optimize Polymorphic Control of Carbamazepine in a CO2 Antisolvent Crystallization Process. *Org. Process Res. Dev.* **2020,** *24* (6), 1006-1017.

115. Dedè, F.; Piccolo, O.; Vigo, D., Dimethyl Fumarate: Heterogeneous Catalysis for the Development of an Innovative Flow Synthesis. *Org. Process Res. Dev.* **2021,** *25* (2), 292-299.

116. Lamberto, D. J.; Neuhaus, J., Robust Process Scale-Up Leveraging Design of Experiments to Map Active Pharmaceutical Ingredient Humid Drying Parameter Space. *Org. Process Res. Dev.* **2021,** *25* (2), 239-249.

117. Al-Dahhan, M. H.; Dudukovic, M. P., Catalyst Bed Dilution for Improving Catalyst Wetting in Laboratory Trickle-Bed Reactors. *AIChE J.* **1996,** *42* (9), 2594-2606.

118. Wang, X.; Abrahams, Q. M.; Zavalij, P. Y.; Doyle, M. P., Highly regio- and stereoselective dirhodium vinylcarbene induced nitrone cycloaddition with subsequent cascade carbenoid aromatic cycloaddition/N-O cleavage and rearrangement. *Angew. Chem. Int. Ed.* **2012,** *51*, 5907-5910.

119. Vaitla, J.; Boni, Y. T.; Davies, H. M. L., Distal Allylic/Benzylic C-H Functionalization of Silyl Ethers Using Donor/Acceptor Rhodium(II) Carbenes. *Angew. Chem. Int. Ed.* **2020,** *59* (19), 7397-7402.

120. Colby, D. A.; Tsai, A. S.; Bergman, R. G.; Ellman, J. A., Rhodium Catalyzed Chelation-Assisted C—H Bond Functionalization Reactions. *Acc. Chem. Res.* **2011,** *45* (6), 814–825.

121. Noisier, A. F.; Brimble, M. A., C-H functionalization in the synthesis of amino acids and peptides. *Chem. Rev.* **2014,** *114* (18), 8775-8806.

122. Hübner, S.; de Vries, J. G.; Farina, V., Why Does Industry Not Use Immobilized Transition Metal Complexes as Catalysts? *Adv. Synth. Catal.* **2016,** *358* (1), 3-25.

123. Duong, U. T.; Gade, A. B.; Plummer, S.; Gallou, F.; Handa, S., Reactivity of Carbenes in Aqueous Nanomicelles Containing Palladium Nanoparticles. *ACS Catal.* **2019,** *9* (12), 10963-10970.

124. Flender, C.; Adams, A. M.; Roizen, J. L.; McNeill, E.; Bois, J. D.; Zare, R. N., Speciation and decomposition pathways of ruthenium catalysts used for selective C–H hydroxylation. *Chem. Sci.* **2014,** *5*, 3309-3314.

125. Mack, J. B. C.; Walker, K. L.; Robinson, S. G.; Zare, R. N.; Sigman, M. S.; Waymouth, R. M.; Du Bois, J., Mechanistic Study of Ruthenium-Catalyzed C-H Hydroxylation Reveals an Unexpected Pathway for Catalyst Arrest. *J. Am. Chem. Soc.* **2019,** *141* (2), 972-980.

126. Gill, C. S.; Venkatasubbaiah, K.; Phan, N. T.; Weck, M.; Jones, C. W., Enhanced cooperativity through design: pendant Co(III)--salen polymer brush catalysts for the hydrolytic kinetic resolution of epichlorohydrin (salen=N,N'-Bis(salicylidene)ethylenediamine dianion). *Chem. Eur. J.* **2008,** *14* (24), 7306-7313.

127. Gill, C. S.; Venkatasubbaiah, K.; Jones, C. W., Recyclable Polymer- and Silica-Supported Ruthenium(II)-Salen Bis-pyridine Catalysts for the Asymmetric Cyclopropanation of Olefins. *Adv. Synth. Catal.* **2009,** *351* (9), 1344-1354.

128. Jain, S.; Venkatasubbaiah, K.; Jones, C. W.; Davis, R. J., Factors influencing recyclability of Co(III)-salen catalysts in the hydrolytic kinetic resolution of epichlorohydrin. *Journal of Molecular Catalysis A: Chemical* **2010,** *316* (1), 8-15.